AIMS Mathematics, 11(4): 11659–11705
DOI: 10.3934/math.2026481
Received: 17 February 2026
Revised: 07 April 2026
Accepted: 20 April 2026
Published: 27 April 2026

https://www.aimspress.com/journal/Math

Research article

Hamiltonian Monte Carlo–based inference for the flexible exponential power–Weibull distribution with applications in reliability analysis

M. G. M. Ghazal[1,2,*]

[1] Department of Mathematics, Faculty of Science, Minia University, Minia 61519, Egypt
[2] University of Technology and Applied Sciences, Rustaq College of Education, Sultanate of Oman

* **Correspondence:** Email: mohamed.gamal@utas.edu.om.

Abstract: In this study, I introduce a new four-parameter lifetime model, termed the flexible exponential power–Weibull (FEPW) distribution, developed by combining the exponential power and Weibull distributions to enhance modeling capability for a wide range of reliability data. The proposed distribution exhibited considerable flexibility in capturing increasing, decreasing, bathtub-shaped, and J-shaped hazard rate behaviors, making it suitable for complex engineering systems. The hazard rate function of the FEPW distribution was derived, and its principal structural properties were rigorously established. Parameter estimation for the FEPW distribution was addressed through maximum likelihood estimation and Bayesian inference. For the Bayesian framework, I implemented Hamiltonian Monte Carlo with the No-U-Turn Sampler (HMC–NUTS) to achieve efficient posterior exploration and stable parameter uncertainty quantification. A detailed simulation study was conducted to evaluate estimator performance under various parameter settings and sample sizes, assessing bias and mean squared error. The practical utility of the proposed model was demonstrated through applications to real-world reliability datasets, where it consistently outperformed several competing lifetime models in terms of goodness-of-fit and information criteria. The results underscored the FEPW distribution as a flexible and useful model for modeling complex failure-time data in reliability engineering and related fields.

Keywords: flexible exponential power–Weibull (FEPW) distribution; bathtub-shaped hazard function; Hamiltonian Monte Carlo; Bayesian inference; lifetime data analysis
Mathematics Subject Classification: 60E05, 62E15, 62E20, 62F10, 62F15

1. Introduction

The field of reliability analysis is fundamental across engineering, manufacturing, finance, and biomedical sciences, where understanding lifetime behavior and failure mechanisms of systems and

components is essential. Accurate modeling of such behavior supports informed decisions regarding system design, preventive maintenance, quality control, and risk assessment. Among lifetime models, the Weibull distribution [1] has long served as a cornerstone due to its flexibility in capturing increasing, decreasing, or constant hazard rate patterns. However, despite its extensive use, the classical Weibull distribution is unable to represent non-monotonic hazard rate functions, most notably the bathtub-shaped curve that characterizes many real-world systems exhibiting early failures, a stable operational phase, and eventual wear–out. This limitation often leads to poor model fit and inadequate characterization of failure dynamics in complex datasets. Consequently, considerable research has focused on extending the Weibull model to overcome its structural constraints and to better accommodate multimodal, modified, and bathtub-shaped hazard behaviors [2, 3].

One widely adopted strategy for constructing more flexible distributions involves compounding or additive mechanisms, in which the hazard rate function (HRF) of the new model is obtained by summing the HRFs of two or more baseline distributions belonging to distinct families. This approach, grounded in competing risks theory, assumes a series system whose lifetime corresponds to the minimum of independent component lifetimes, resulting in a combined HRF that inherits flexibility from its constituents. Additive models prove particularly effective when integrating distributions with complementary hazard patterns. Several lifetime distributions have been developed to improve modeling flexibility in reliability analysis. For instance, Singh [4] proposed an additive Perks–Weibull model with bathtub-shaped hazard behavior, while Shakhatreh et al. [5] introduced the log-normal modified Weibull distribution and discussed its reliability implications. In addition, Abba et al. [6] developed a reliability and survival model for one- and two-failure-mode systems, and Méndez-González et al. [7] studied the Chen–Perks distribution with emphasis on reliability properties. More recent contributions have focused on robust bathtub-shaped failure-time models and Bayesian reliability inference under flexible hazard structures [8, 9].

The Additive Weibull (AW) distribution, proposed by Jiang and Murthy [10], combines two Weibull components in a competing-risk structure, resulting in a four-parameter model with hazard function

$$h(x) = abx^{b-1} + cdx^{d-1}.$$

This formulation effectively captures bathtub-shaped hazard functions and has demonstrated superior fitting performance over the classical Weibull in real datasets. The Weibull–modified Weibull (WMW) distribution (Almalki and Yuan [11]) extends this approach by compounding a Weibull with a modified Weibull, yielding a five-parameter distribution capable of modeling more complex bathtub-shaped structures, with maximum likelihood estimation (MLE) showing strong empirical performance. The additive Perks–Weibull distribution (Singh [4]) sums the Perks and Weibull hazard functions, producing a flexible four-parameter model particularly useful for datasets exhibiting short useful-life periods or competing failure modes. A novel lifetime distribution, termed the Weibull–Chen distribution [12], was proposed by integrating the Weibull and Chen distributions to effectively model lifetime data exhibiting bathtub-shaped hazard rates. The results demonstrated its superior flexibility and improved fit to real-world lifetime datasets compared to existing models. Independently, Thach and Bris [13] developed an equivalent model, named the additive Chen–Weibull (ACW) distribution, which combines the HRFs of the Chen and Weibull distributions into a flexible four-parameter framework capable of accommodating increasing and bathtub-shaped hazards. Parameter estimation was performed using MLE, bootstrap confidence intervals (CIs), and Bayesian inference via

Hamiltonian Monte Carlo (HMC). The additive Gompertz–Weibull distribution [14] further enhances flexibility by combining exponential growth behavior (Gompertz) with Weibull aging patterns, showing strong performance under Bayesian HMC inference. Moreover, the Flexible Dhillon–Weibull distribution (Abba et al. [15]) merged the Dhillon and Weibull families to accommodate monotone and non-monotone hazard shapes, including decreasing, upside-down bathtub, and modified bathtub curves, with Bayesian HMC offering precise parameter inference.

Despite these advancements, several challenges remain in some current hybrid Weibull-based lifetime models. A primary limitation concerns restricted hazard-rate flexibility: Some distributions struggle to represent all phases of the bathtub curve–particularly accurate identification of change points and the flat useful-life region-or fail to adequately model multimodal behaviors. A second challenge arises in Bayesian inference, where non-conjugacy and high-dimensional parameter spaces lead to slow mixing, low acceptance rates, and convergence difficulties in traditional Markov chain Monte Carlo algorithms such as Metropolis-Hastings. A further constraint is the inability of many standard Weibull extensions to effectively model heavy-tailed data or accommodate varying degrees of kurtosis. This rigidity makes them less suitable for datasets containing outliers or representing systems subject to random external shocks, where the probability of extreme failure times is higher than what classical models predict. These challenges underscore the need for more flexible, computationally efficient, and analytically tractable models.

To address these limitations, this study introduces the flexible exponential power–Weibull (FEPW) distribution, a novel four-parameter model constructed by compounding the exponential power and Weibull distributions. The FEPW distribution provides an exceptionally adaptable framework for lifetime modeling, capable of representing increasing, decreasing, J-shaped, and full bathtub-shaped hazard functions with smoothly transitioning phases and an identifiable plateau in the useful-life region.

The significance of the FEPW distribution lies not only in its flexibility but also in its statistical robustness. Unlike many competing hybrid models constrained by rigid tail behaviors, the proposed FEPW framework effectively accommodates heavy-tailed data and varying degrees of kurtosis via the exponential power component. This structural advantage enables the precise modeling of systems subject to random external shocks or extreme failure events (outliers), offering a distinct physical justification for its use in complex engineering contexts. Furthermore, the study implemented a robust dual-estimation strategy. While Maximum Likelihood Estimation (MLE) proved effective for large datasets, the Bayesian framework utilizing HMC–NUTS demonstrated superior stability and precision in small-sample scenarios, successfully mitigating the challenges of the high-dimensional parameter space.

The remainder of this article is organized as follows: In Section 2, I introduce the FEPW distribution and discuss its hazard-rate behavior. In Section 3, I present its mathematical and reliability properties, including moments, entropy, mean time to failure, and stress—strength reliability. In Section 4, I describe parameter estimation using MLE and Bayesian HMC–NUTS. In Section 5, I report simulation studies evaluating estimator performance. In Section 6, I apply the FEPW model to real-world datasets and compare it with competing distributions. Finally, in Section 7, I conclude with key findings and directions for future research.

2. The flexible exponential power–Weibull (FEPW) distribution

In this section, I introduce the proposed flexible exponential power–Weibull (FEPW) distribution, detail its core functions, and provide a comprehensive analysis of its HRF behavior. The FEPW is built using a competing risks framework, where the observed lifetime X represents the minimum of two independent latent failure times from distinct distributional families.

Let U_1 follow an exponential power (EP) distribution with reliability function (RF):

$$R_{U_1}(u_1) = \mathrm{e}^{1-\mathrm{e}^{(\tau u_1)^\eta}}, \qquad u_1 > 0,$$

with shape parameter $\eta > 0$ and scale parameter $\tau \geq 0$. Similarly, let U_2 follow a Weibull distribution with RF:

$$R_{U_2}(u_2) = \mathrm{e}^{-(\kappa u_2)^\varphi}, \qquad u_2 > 0,$$

where $\varphi > 0$ is a shape parameter and $\kappa \geq 0$ is a scale parameter.

Assuming independence between U_1 and U_2, the FEPW random variable is defined as $X = \min(U_1, U_2)$, which corresponds to a series system subject to two independent failure modes. Consequently, $X \sim \mathrm{FEPW}(\Theta)$, with parameter vector $\Theta = (\tau, \eta, \kappa, \varphi)$.

Under this construction, the RF of X is the product of the individual RFs:

$$R(x;\Theta) = P(X > x) = \prod_{i=1}^{2} R_{U_i}(u_i) = \mathrm{e}^{1-\mathrm{e}^{(\tau x)^\eta}-(\kappa x)^\varphi}, \qquad x > 0, \tag{2.1}$$

where $\eta, \varphi > 0$ are shape parameters controlling the distribution's behavior, while $\tau, \kappa \geq 0$ are scale parameters. From the RF in Eq (2.1), the cumulative distribution function (CDF) of the FEPW distribution is obtained as

$$F(x;\Theta) = 1 - \mathrm{e}^{1-\mathrm{e}^{(\tau x)^\eta}-(\kappa x)^\varphi}. \tag{2.2}$$

The corresponding probability density function (PDF) of the proposed model is obtained as:

$$f(x;\Theta) = \left(\eta\,\tau\,(\tau x)^{\eta-1}\,\mathrm{e}^{(\tau x)^\eta} + \kappa\,\varphi\,(\kappa x)^{\varphi-1}\right)\mathrm{e}^{1-\mathrm{e}^{(\tau x)^\eta}-(\kappa x)^\varphi}. \tag{2.3}$$

Finally, the HRF, a critical measure in reliability analysis, is derived as

$$h(x;\Theta) = \eta\,\tau\,(\tau x)^{\eta-1}\,\mathrm{e}^{(\tau x)^\eta} + \kappa\,\varphi\,(\kappa x)^{\varphi-1}. \tag{2.4}$$

2.1. Identifiability of the FEPW distribution

Before proceeding to statistical inference, I note that the parameterization of the FEPW distribution is identifiable.

Proposition 1. Let $\Theta_1 = (\tau_1, \eta_1, \kappa_1, \varphi_1)$ and $\Theta_2 = (\tau_2, \eta_2, \kappa_2, \varphi_2)$ be two parameter vectors of the FEPW distribution. If

$$R(x;\Theta_1) = R(x;\Theta_2), \qquad \forall x > 0,$$

then $\Theta_1 = \Theta_2$.

Proof. From Eq (2.1), the equality $R(x;\Theta_1) = R(x;\Theta_2)$ implies

$$\mathrm{e}^{(\tau_1 x)^{\eta_1}} + (\kappa_1 x)^{\varphi_1} = \mathrm{e}^{(\tau_2 x)^{\eta_2}} + (\kappa_2 x)^{\varphi_2}, \qquad \forall x > 0.$$

Using the expansion

$$e^{(\tau x)^\eta} = 1 + (\tau x)^\eta + o(x^\eta), \qquad x \to 0,$$

the smallest nonzero power of x on each side uniquely determines the smaller of η and κ, with its corresponding coefficient. After subtracting this leading term, the remaining term determines the second exponent and coefficient. Hence, when $\eta \neq \varphi$, all four parameters are uniquely identified.

In the special case $\eta = \varphi = r$, the above identity becomes

$$e^{(\tau_1 x)^r} + (\kappa_1 x)^r = e^{(\tau_2 x)^r} + (\kappa_2 x)^r.$$

As $x \to \infty$, the exponential term dominates the polynomial term, which yields $\tau_1 = \tau_2$, and the common exponent is the same on both sides. Substituting back then gives $(\kappa_1 x)^r = (\kappa_2 x)^r$ for all $x > 0$, and therefore $\kappa_1 = \kappa_2$. Thus, $\Theta_1 = \Theta_2$.

Therefore, the FEPW distribution is identifiable, and the case $\tau = \kappa$ and $\eta = \varphi$ corresponds only to a nested submodel, not to a lack of parameter identifiability. □

2.2. Shapes of the hazard rate function (HRF)

The HRF is a fundamental tool in lifetime and reliability analysis, as it characterizes the instantaneous risk of failure at time x, given survival up to that time. Understanding its shape is essential because systems exhibit markedly different reliability behaviors depending on whether failure risks increase, decrease, or vary non-monotonically over time. The proposed FEPW distribution provides substantial flexibility in this regard, enabling it to accommodate a wide spectrum of hazard-rate structures driven by the interaction between the exponential power and Weibull components. For many extended lifetime models, including the proposed FEPW distribution, the HRF shape can be analytically examined. As given in Eq (2.4), the HRF of the FEPW distribution exhibits an increasing pattern when both shape parameters satisfy $\eta > 1$ and $\varphi > 1$. Conversely, it displays a decreasing pattern when $0 < \eta < 1$ and $0 < \varphi < 1$. Notably, the bathtub shape, a key feature for modeling real-world systems with infant mortality, useful life, and wear-out phases, arises when one shape parameter exceeds 1 and the other is less than 1 (i.e., $\eta > 1 > \varphi$ or $\varphi > 1 > \eta$).

More formally, the bathtub shape manifests if there exists a critical point $x = x^*$ where the first derivative of the HRF, $h'(x; \Theta)$, equals zero:

$$h'(x; \Theta) = \eta\tau^\eta (x^*)^{\eta-2} \left(\eta\left((\tau x^*)^\eta + 1\right) - 1\right) e^{(\tau x^*)^\eta} + (\varphi - 1)\varphi\kappa^\varphi (x^*)^{\varphi-2} = 0.$$

The HRF is decreasing for $x < x^*$ if $h'(x; \Theta) < 0$ and increasing for $x > x^*$ if $h'(x; \Theta) > 0$, confirming the bathtub configuration. This versatility positions the FEPW distribution as a robust tool for diverse reliability scenarios involving non-monotonic failure risks.

Figures 1 and 2 illustrate the flexibility of the FEPW distribution. Figure 1 displays various shapes of its PDF, including unimodal, decreasing, and modified bathtub forms. Figure 2 presents the corresponding HRFs under different parameter settings, demonstrating its ability to model increasing, decreasing, and bathtub-shaped failure patterns, some with extended plateaus in the useful-life phase.

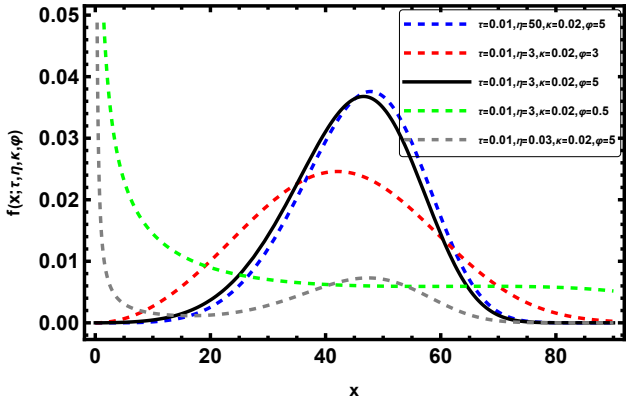

Figure 1. PDFs of the FEPW distribution for selected parameter values.

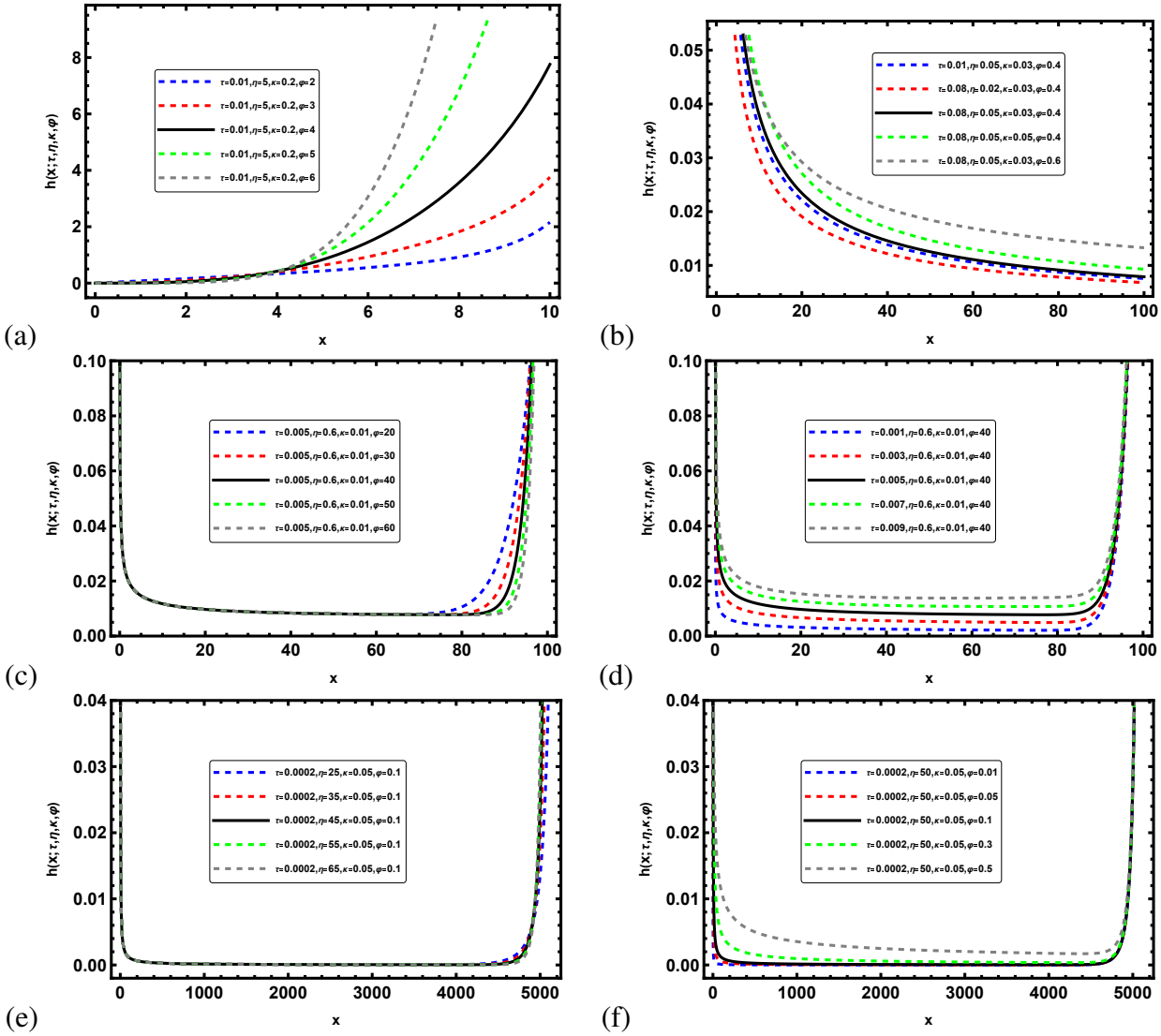

Figure 2. HRFs of the FEPW distribution under various parameter configurations.

3. Properties of the FEPW distribution

In this section, I derive several fundamental statistical properties of the FEPW distribution, including the mode, quantile function, moments, incomplete moments, mean residual life (MRL), mean time to failure (MTTF), Rényi entropy, Mills ratio, stress-strength reliability, and order statistics. These properties provide essential insights into the distribution's behavior, facilitating its application in reliability engineering, survival analysis, and risk assessment.

3.1. Mode

The mode of the FEPW distribution is found by setting the first derivative of the PDF in Eq (2.3) to zero, yielding:

$$\left(-\eta^2\tau^{2\eta}x^{2\eta-2}\mathrm{e}^{2(\tau x)^\eta}+\eta\tau^\eta x^{\eta-2}\mathrm{e}^{(\tau x)^\eta}\left(\eta+\eta(\tau x)^\eta-2\varphi(\kappa x)^\varphi-1\right)-\varphi\kappa^\varphi x^{\varphi-2}\left(\varphi\left((\kappa x)^\varphi-1\right)+1\right)\right)$$
$$\times\,\mathrm{e}^{-\mathrm{e}^{(\tau x)^\eta}-(\kappa x)^\varphi+1}=0.$$

This equation lacks a closed-form solution, necessitating numerical methods in specialized software (e.g., Wolfram Mathematica or R) for approximation.

3.2. Quantile function

The quantile function plays a pivotal role in data simulation, robust estimation, and constructing CIs. It enables the generation of random samples from the distribution. In reliability engineering, it enables the determination of critical thresholds, such as the time by which a specified proportion of failures is expected, supporting warranty analysis and quality control.

The p-th quantile x_q of the FEPW distribution, derived from Eq (2.2), satisfies:

$$\mathrm{e}^{(\tau\,x_q)^\eta}+(\kappa\,x_q)^\varphi=1-\ln(1-q),\quad 0<q<1. \tag{3.1}$$

This equation is solved numerically to obtain quantile values.

3.3. Moments

Moments provide essential information about the distribution's shape, spread, and central tendency. The r-th moment is particularly important for calculating the mean, variance, skewness, and kurtosis, which are critical for understanding failure time characteristics.

Theorem 1. *Let $X\sim FEPW(\Theta)$. Then, the r-th raw moment of X, denoted by μ_r, for $r=1,2,\ldots$, is given by*

$$\mu_r=r\,\mathrm{e}\sum_{i=0}^{+\infty}\sum_{j=0}^{+\infty}\frac{(-1)^i\,i^j\,\tau^{j\eta}}{i!\,j!\,\varphi\,\kappa^{r+j\eta}}\Gamma\left(\frac{r+j\eta}{\varphi}\right), \tag{3.2}$$

where $\Gamma(\cdot)$ is the gamma function.

Proof. See Appendix A.1. □

3.4. Incomplete moments

Theorem 2. *The r-th incomplete moment of the FEPW distribution $I_m^r(v)$, is*

$$I_m^r(v) = \mathrm{e}\sum_{i=0}^{+\infty}\sum_{j=0}^{+\infty}\sum_{k=0}^{+\infty}\frac{(-1)^i i^j \tau^{(k+j+1)\eta}\,\eta}{i!\,j!k!\,\varphi\,\kappa^{r+(1+j+k)\eta}}\,\gamma_1\left(\frac{r+(1+j+k)\eta}{\varphi},\,(\kappa\,v)^{\varphi}\right)$$

$$+\,\mathrm{e}\sum_{i=0}^{+\infty}\sum_{j=0}^{+\infty}\frac{(-1)^i i^j \tau^{j\eta}}{i!\,j!\,\kappa^{r+j\eta}}\,\gamma_2\left(\frac{r+j\eta}{\varphi}+1,\,(\kappa\,v)^{\varphi}\right), \tag{3.3}$$

where $\gamma(s,z)=\int_0^z t^{s-1}e^{-t}\,dt$ is the lower incomplete gamma function.

Proof. See Appendix A.2. □

3.5. Mean residual life

The MRL quantifies the expected remaining lifetime given survival to a certain time, serving as a dynamic reliability indicator. It is vital for scheduling maintenance in aging systems and for optimizing replacement policies in industries like aviation and manufacturing, where underestimating residual life can lead to costly failures.

Theorem 3. *The MRL of the FEPW distribution is*

$$\mu_X(t)=\mathrm{e}^{\mathrm{e}^{(\tau\,t)^{\eta}}+(\kappa\,t)^{\varphi}}\sum_{i=0}^{+\infty}\sum_{j=0}^{+\infty}\frac{(-1)^i\,i^j\,\tau^{j\eta}}{i!\,j!\,\varphi\,\kappa^{j\eta+1}}\,\Gamma\Big(\frac{j\eta+1}{\varphi},\,(\kappa\,t)^{\varphi}\Big), \tag{3.4}$$

where $\Gamma(s,z)=\int_z^{\infty} t^{s-1}e^{-t}\,dt$ is the upper incomplete gamma function.

Proof. See Appendix A.3. □

3.6. Mean time to failure

The MTTF is a fundamental reliability metric representing the expected operational period before system failure, which is essential for product quality assessment and system design. The MTTF is obtained from the first raw moment in Theorem 1 by setting $r=1$:

$$\mathrm{MTTF}=\mathrm{e}\sum_{i=0}^{+\infty}\sum_{j=0}^{+\infty}\frac{(-1)^i\,i^j\,\tau^{j\eta}}{i!\,j!\,\varphi\,\kappa^{j\eta+1}}\Gamma\left(\frac{j\eta+1}{\varphi}\right).$$

Table 1 presents Monte Carlo estimates of the MRL at selected time points and the MTTF under two parameter settings of the FEPW distribution, along with their corresponding MSEs. The MRL values decrease with increasing t, which is consistent with the expected aging behavior of lifetime models. As anticipated, the identity MTTF = $\mathrm{MRL}(t)|_{t=0}$ holds numerically, confirming the internal coherence of the proposed expressions. Across all sample sizes, the MSEs exhibit a downward trend, demonstrating increasing estimator precision, while MTTF estimates remain stable and close to their true values, underscoring the robustness of the FEPW distribution.

Table 1. Monte Carlo estimates of MRL at selected time points and the MTTF for two parameter settings of the FEPW distribution with their corresponding MSEs.

n	MRL at time t					MTTF
	$t = 0.01$	$t = 0.25$	$t = 0.65$	$t = 0.95$	$t = 1.4$	
$\tau = 0.6, \eta = 6, \kappa = 0.04, \varphi = 0.4$						
30	1.20393 (0.09825)	1.0955 (0.06999)	0.76876 (0.05289)	0.51433 (0.04371)	0.18984 (0.02898)	1.16368 (0.10576)
75	1.1994 (0.06118)	1.09583 (0.04534)	0.76977 (0.03288)	0.51283 (0.02847)	0.19054 (0.01852)	1.1583 (0.06554)
150	1.20038 (0.04233)	1.09581 (0.0312)	0.76938 (0.02328)	0.51332 (0.01931)	0.19003 (0.01314)	1.15919 (0.04495)
230	1.20085 (0.03514)	1.09603 (0.02501)	0.77013 (0.01901)	0.51407 (0.01576)	0.19013 (0.01064)	1.1595 (0.03757)
300	1.20222 (0.03072)	1.09648 (0.02237)	0.77032 (0.01683)	0.51375 (0.01376)	0.19030 (0.00948)	1.1604 (0.0326)
400	1.20148 (0.02661)	1.0969 (0.01971)	0.7697 (0.01451)	0.51291 (0.01194)	0.19022 (0.00807)	1.1599 (0.02849)
500	1.20049 (0.02337)	1.0967 (0.01776)	0.77032 (0.01332)	0.5135 (0.01079)	0.19048 (0.00726)	1.15922 (0.02477)
$\tau = 0.05, \eta = 0.8, \kappa = 0.7, \varphi = 8.5$						
30	1.25670 (0.05846)	1.04529 (0.05013)	0.68086 (0.03857)	0.40756 (0.03295)	0.11541 (0.02504)	1.26347 (0.05972)
75	1.25443 (0.03766)	1.04744 (0.03079)	0.67889 (0.02494)	0.40812 (0.02079)	0.11591 (0.01589)	1.26107 (0.03824)
150	1.25446 (0.02657)	1.04626 (0.02145)	0.67979 (0.01795)	0.40714 (0.01521)	0.11549 (0.01103)	1.26135 (0.02714)
230	1.25491 (0.02156)	1.04627 (0.01723)	0.67926 (0.01391)	0.40787 (0.01225)	0.11555 (0.00888)	1.26157 (0.02175)
300	1.25431 (0.01893)	1.04734 (0.01543)	0.67954 (0.01239)	0.40754 (0.01068)	0.11616 (0.00767)	1.26112 (0.01933)
400	1.25503 (0.01621)	1.04665 (0.01316)	0.67903 (0.01073)	0.40728 (0.00942)	0.11583 (0.00682)	1.26165 (0.01653)
500	1.25484 (0.01475)	1.04689 (0.01234)	0.67933 (0.00954)	0.40711 (0.00823)	0.11576 (0.00597)	1.26162 (0.01497)

Figure 3 illustrates the MSE trajectories for MRL and MTTF. In each parameter configuration, the MSE curves decline steadily as n increases, with the largest improvements occurring when transitioning from small to moderate sample sizes. Beyond that range, reductions in MSE become more gradual, reflecting diminishing marginal gains and aligning with theoretical asymptotic behavior. These patterns confirm the efficiency and reliability of the estimation methodology for the FEPW distribution.

Figure 4 displays the trace plots and posterior density estimates for MRL and MTTF. The trace plots exhibit rapid mixing and stationarity, with no drift or autocorrelation patterns, indicating successful convergence. The posterior densities are smooth, unimodal, and concentrated around the Monte Carlo means, providing strong evidence of estimator consistency and the reliability of the simulation procedure.

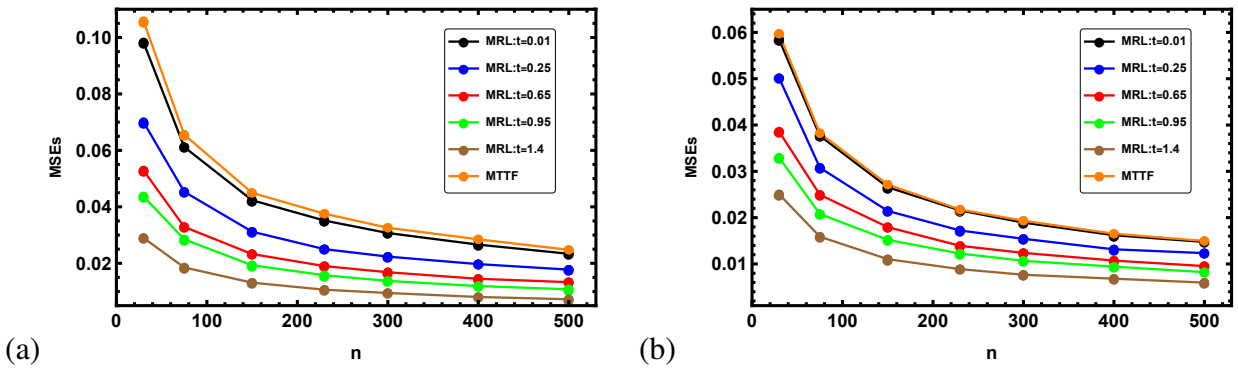

Figure 3. MSE trajectories of the estimated MRL and MTTF for the FEPW distribution across sample sizes under two parameter configurations.

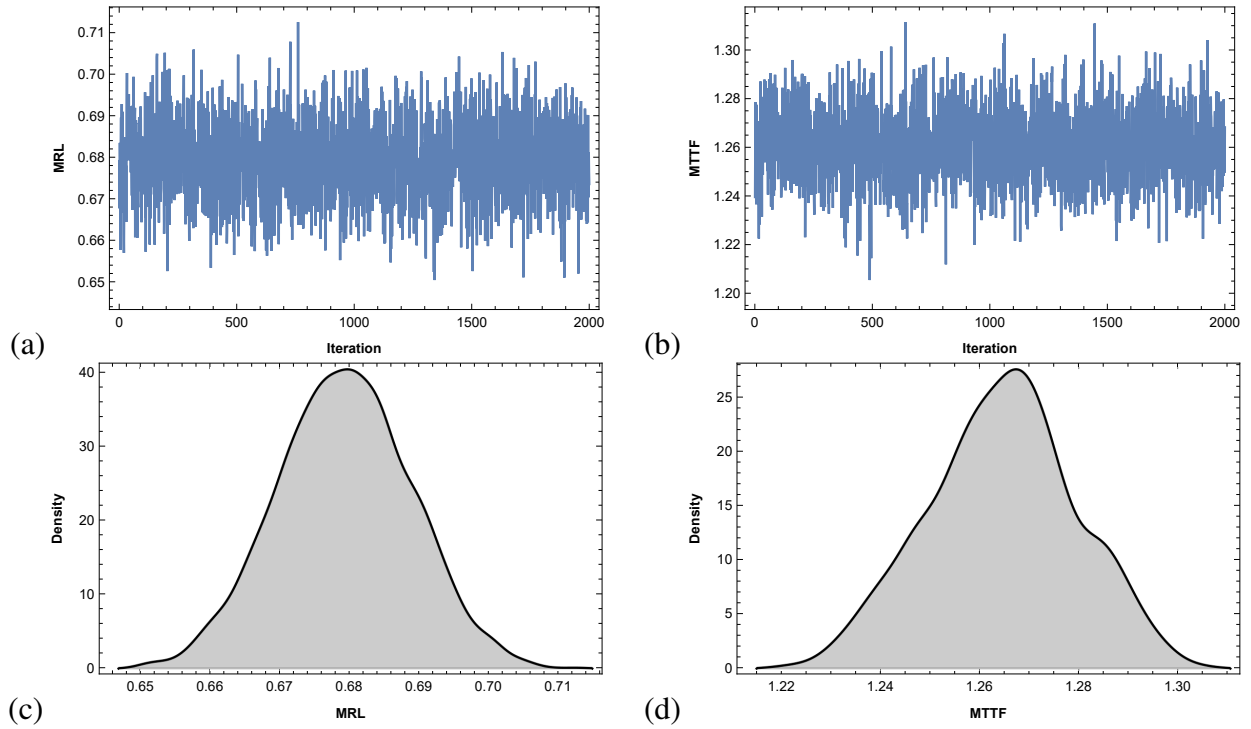

Figure 4. Trace plots and posterior density estimates of the MRL and MTTF obtained from a Monte Carlo simulation for the FEPW distribution with a sample size of $n = 500$ and at time $t = 0.65$, under the parameter setting $\tau = 0.05, \eta = 0.8, \kappa = 0.7$, and $\varphi = 8.5$.

3.7. Rényi entropy

Rényi entropy quantifies the uncertainty or randomness in a system, with applications in information theory, reliability engineering, and risk assessment.

Theorem 4. *For order r ($r > 0$, $r \neq 1$), the Rényi entropy $H_r(X)$ of the FEPW distribution can be written as*

$$H_r(X) = \frac{1}{1-r} \log \sum_{j=0}^{+\infty} \sum_{k=0}^{+\infty} \sum_{l=0}^{+\infty} \sum_{i=0}^{r} \frac{\binom{r}{i} e^r (-1)^k i^j r^k k^l \tau^{(i+j+l)\eta} \eta^i \kappa^{(r-i)\varphi} \varphi^{(r-i-1)}}{j!\, k!\, l!\, (r\kappa^{\varphi})^{\frac{(i+j+l)\eta+(r-i)\varphi-r+1}{\varphi}}}$$
$$\times \Gamma\left(\frac{(i+j+l)\eta + (r-i)\varphi - r + 1}{\varphi}\right). \tag{3.5}$$

Proof. See Appendix A.4. □

3.8. Mills ratio

The Mills ratio links the RF and the hazard rate, providing a measure of tail behavior. It is frequently used in extreme value theory and censoring models.

For the FEPW distribution, the Mills ratio is defined as:

$$M(x;\Theta) = \frac{R(x;\Theta)}{f(x;\Theta)}$$

$$= \frac{1}{\eta\,\tau\,(\tau x)^{\eta-1}\,\mathrm{e}^{(\tau x)^{\eta}} + \kappa\,\varphi\,(\kappa\,x)^{\varphi-1}}.$$

3.9. Stress-strength reliability

Stress-strength reliability measures the probability that a system's strength exceeds applied stress, a critical metric in engineering design and reliability assessment.

Theorem 5. *Let $X \sim FEPW(\Theta_1)$ denote strength and $Y \sim FEPW(\Theta_2)$ denote stress, with X and Y independent. Then, the reliability $R_{SS} = P(X > Y)$ is:*

$$\begin{aligned} R_{SS} &= \mathrm{e}^2 \sum_{i=0}^{+\infty}\sum_{j=0}^{+\infty}\sum_{k=0}^{+\infty}\sum_{l=0}^{+\infty}\sum_{m=0}^{+\infty}\sum_{n=0}^{+\infty} \frac{(-1)^{i+k+l} i^j l^m \tau_1^{j\eta_1} \kappa_1^{k\varphi_1} \tau_2^{m\eta_2}}{i!\,j!\,k!\,l!\,m!\,n!\,\varphi_2\,\kappa_2^{j\eta_1+k\varphi_1+(m+n+1)\eta_2}} \Gamma\left(\frac{j\eta_1 + k\varphi_1 + (m+n+1)\eta_2}{\varphi_2}\right) \\ &\quad + \mathrm{e}^2 \sum_{i=0}^{+\infty}\sum_{j=0}^{+\infty}\sum_{k=0}^{+\infty}\sum_{l=0}^{+\infty}\sum_{m=0}^{+\infty} \frac{(-1)^{i+k+l} i^j l^m \tau_1^{j\eta_1} \kappa_1^{k\varphi_1} \tau_2^{m\eta_2}}{i!\,j!\,k!\,l!\,m!\,\kappa_2^{j\eta_1+k\varphi_1+m\eta_2}} \Gamma\left(\frac{j\eta_1 + k\varphi_1 + m\eta_2}{\varphi_2} + 1\right). \end{aligned} \tag{3.6}$$

Proof. See Appendix A.5. □

3.10. Order statistics

Order statistics are essential for understanding extreme values and system reliability, particularly in quality control and failure analysis where the minimum or maximum lifetimes are of interest.

Theorem 6. *Let $X_{1:n} \le X_{2:n} \le \cdots \le X_{n:n}$ denote the order statistics from a random sample of size n from the FEPW distribution. The PDF of the k-th order statistic $X_{k:n}$ is*

$$f_{k:n}(x;\Theta) = \frac{n!}{(n-k)!}\,h(x;\Theta)\sum_{j=0}^{k-1}\frac{(-1)^j}{j!\,(k-j-1)!}\,[R(x;\Theta)]^{n-k+j+1}.$$

where $h(x;\Theta)$ and $R(x;\Theta)$ are the HRF and RF of the FEPW distribution, respectively.

Proof. See Appendix A.6. □

All proofs are provided in Appendix A, utilizing series expansions and integral transformations to establish these fundamental properties of the FEPW distribution.

Remark. The infinite-series representations derived for moments, entropy, and stress-strength reliability are absolutely convergent for all admissible parameter values $\tau > 0$, $\eta > 0$, $\kappa > 0$, and $\varphi > 0$. This convergence follows from the exponential-series expansion together with the factorial terms in the denominators, which dominate the polynomial growth in the numerators. Consequently, these analytical expressions remain well-defined and numerically stable throughout the parameter space.

For numerical evaluation, the infinite sums are truncated at sufficiently large indices, and truncation stability is verified by increasing the truncation levels until successive approximations changed negligibly. For Eq (3.2), numerical verification in *Mathematica* show that the truncated double series stabilizes rapidly and achieves accuracy within 10^{-6} at truncation level $i_{\max} = j_{\max} = 20$, with final approximation $\mu_r \approx 26.1647$. The detailed numerical values are reported in Table 2, while the corresponding stabilization trend and successive absolute changes are illustrated in Figure 5. The computed value remains unchanged under further truncation refinement.

Table 2. Truncation stability of the series representation in Eq (3.2) for selected truncation levels $i_{\max} = j_{\max}$.

Truncation level ($i_{\max} = j_{\max}$)	Approximation of μ_r	Absolute change
5	23.2899	–
10	26.1660	2.87614
15	26.1647	0.00132322
20	26.1647	8.63983×10^{-8}
25	26.1647	5.28644×10^{-12}
30	26.1647	1.42109×10^{-14}
35	26.1647	3.55271×10^{-15}
40	26.1647	0
45	26.1647	0
50	26.1647	0

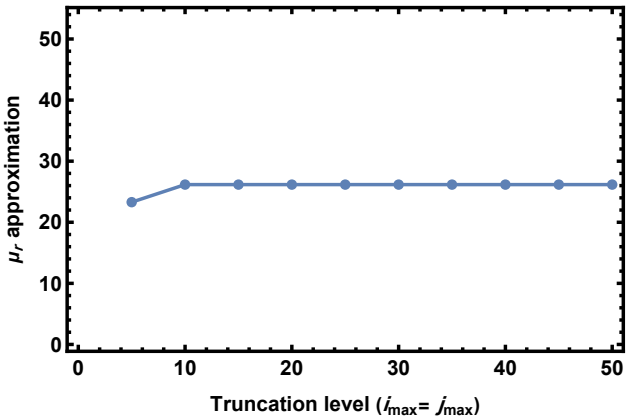

(a) Truncation stability of Eq (3.2).

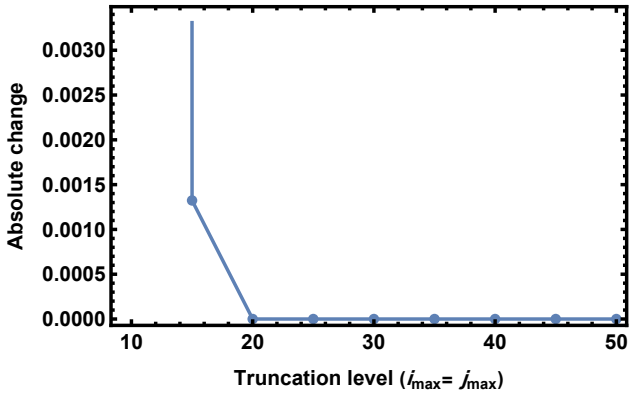

(b) Successive absolute changes in the truncated approximations.

Figure 5. Numerical truncation stability analysis for Eq (3.2) with common truncation levels $i_{\max} = j_{\max}$.

4. Parameter estimation

In this section, I detail the methodologies for estimating the parameters of the FEPW distribution, encompassing classical and Bayesian paradigms. The MLE method is employed to derive point estimates and construct asymptotic CIs. For the Bayesian approach, I utilize the HMC algorithm, focusing on its adaptive variant, the NUTS, which offers an efficient framework for exploring complex posterior distributions.

4.1. Maximum likelihood estimation

Let $\boldsymbol{\Theta} = (\tau, \eta, \kappa, \varphi)$ denote the parameter vector and $\underline{\mathbf{x}} = \{x_1, \ldots, x_n\}$ be an independent and identically distributed (i.i.d.) sample from FEPW($\boldsymbol{\Theta}$). The likelihood function $L(\boldsymbol{\Theta})$ is expressed as

$$L(\Theta) = \prod_{i=1}^{n} \left(\tau\eta(\tau x_i)^{\eta-1} \mathrm{e}^{(\tau x_i)^{\eta}} + \kappa\varphi(\kappa x_i)^{\varphi-1} \right) e^{\sum_{i=1}^{n} \left(1 - e^{(\tau x_i)^{\eta}} - (\kappa x_i)^{\varphi}\right)}. \tag{4.1}$$

The log-likelihood becomes

$$\ell(\boldsymbol{\Theta}) = \sum_{i=1}^{n} \log\left(\tau\eta(\tau x_i)^{\eta-1}\mathrm{e}^{(\tau x_i)^{\eta}} + \kappa\varphi(\kappa x_i)^{\varphi-1}\right) + \sum_{i=1}^{n}\left(1 - \mathrm{e}^{(\tau x_i)^{\eta}} - (\kappa x_i)^{\varphi}\right). \tag{4.2}$$

The MLEs $\hat{\boldsymbol{\Theta}} = (\hat{\tau}, \hat{\eta}, \hat{\kappa}, \hat{\varphi})$ are obtained by solving the system of score equations:

$$\begin{aligned}
\frac{\partial \ell(\boldsymbol{\Theta})}{\partial \tau} &= \frac{\eta^2}{\tau}\sum_{i=1}^{n}\frac{(\tau x_i)^{\eta}\left((\tau x_i)^{\eta}+1\right)e^{(\tau x_i)^{\eta}}}{\eta(\tau x_i)^{\eta}e^{(\tau x_i)^{\eta}} + \varphi(\kappa x_i)^{\varphi}} - \frac{\eta}{\tau}\sum_{i=1}^{n}(\tau x_i)^{\eta}e^{(\tau x_i)^{\eta}} = 0,\\
\frac{\partial \ell(\boldsymbol{\Theta})}{\partial \eta} &= \sum_{i=1}^{n}\frac{(\tau x_i)^{\eta}\left(\eta\left((\tau x_i)^{\eta}+1\right)\log(\tau x_i)+1\right)e^{(\tau x_i)^{\eta}}}{\eta e^{(\tau x_i)^{\eta}}(\tau x_i)^{\eta} + \varphi(\kappa x_i)^{\varphi}} - \sum_{i=1}^{n}(\tau x_i)^{\eta}\log(\tau x_i)\,e^{(\tau x_i)^{\eta}} = 0,\\
\frac{\partial \ell(\boldsymbol{\Theta})}{\partial \kappa} &= \frac{\varphi^2}{\kappa}\sum_{i=1}^{n}\frac{1}{\eta(\tau x_i)^{\eta}(\kappa x_i)^{-\varphi}e^{(\tau x_i)^{\eta}} + \varphi} - \frac{\varphi}{\kappa}\sum_{i=1}^{n}(\kappa x_i)^{\varphi-1} = 0,\\
\frac{\partial \ell(\boldsymbol{\Theta})}{\partial \varphi} &= \sum_{i=1}^{n}\frac{(\kappa x_i)^{\varphi}\left(\varphi\log(\kappa x_i)+1\right)}{\eta e^{(\tau x_i)^{\eta}}(\tau x_i)^{\eta} + \varphi(\kappa x_i)^{\varphi}} - \sum_{i=1}^{n}(\kappa x_i)^{\varphi}\log(\kappa x_i) = 0.
\end{aligned}$$

The explicit forms of these score equations are complex and do not yield closed-form solutions. Therefore, numerical optimization algorithms, such as the Newton-Raphson method or other iterative techniques available in statistical software packages (e.g., `FindMaximum` in Mathematica, `optim` in R), must be employed to obtain the estimates.

Under mild regularity conditions, the MLE vector $\hat{\boldsymbol{\Theta}}$ follows an asymptotic multivariate normal distribution for large n, with mean $\boldsymbol{\Theta}$ and variance–covariance matrix equal to the inverse of the Fisher information matrix. In practice, the observed Fisher information matrix (FIM) $\mathbf{I}(\hat{\boldsymbol{\Theta}})$ is approximated by the negative Hessian matrix of the log-likelihood evaluated at $\hat{\boldsymbol{\Theta}}$:

$$\mathbf{I}(\widehat{\Theta}) = -\begin{bmatrix}
\frac{\partial^2\ell(\boldsymbol{\Theta})}{\partial\tau^2} & \frac{\partial^2\ell(\boldsymbol{\Theta})}{\partial\tau\partial\eta} & \frac{\partial^2\ell(\boldsymbol{\Theta})}{\partial\tau\partial\kappa} & \frac{\partial^2\ell(\boldsymbol{\Theta})}{\partial\tau\partial\varphi}\\
\cdot & \frac{\partial^2\ell(\boldsymbol{\Theta})}{\partial\eta^2} & \frac{\partial^2\ell(\boldsymbol{\Theta})}{\partial\eta\partial\kappa} & \frac{\partial^2\ell(\boldsymbol{\Theta})}{\partial\eta\partial\varphi}\\
\cdot & \cdot & \frac{\partial^2\ell(\boldsymbol{\Theta})}{\partial\kappa^2} & \frac{\partial^2\ell(\boldsymbol{\Theta})}{\partial\kappa\partial\varphi}\\
\cdot & \cdot & \cdot & \frac{\partial^2\ell(\boldsymbol{\Theta})}{\partial\varphi^2}
\end{bmatrix}_{\boldsymbol{\Theta}=\widehat{\Theta}},$$

where the elements indicated by '·' are filled by symmetry. The formulas for these second partial derivatives are extensive and provided in Appendix B.

The estimated variance–covariance matrix is then $\widehat{\mathrm{Var}}(\hat{\boldsymbol{\Theta}}) = \mathbf{I}(\hat{\boldsymbol{\Theta}})^{-1}$. An approximate $100(1-\zeta)\%$ CI for parameter Θ_j ($j \in \{\tau, \eta, \kappa, \varphi\}$) is

$$\hat{\Theta}_j \pm z_{\zeta/2}\sqrt{\widehat{\mathrm{Var}}(\hat{\Theta}_{jj})}, \qquad j \in \{\tau, \eta, \kappa, \varphi\},$$

where $z_{\zeta/2}$ is the $\zeta/2$-quantile of the standard normal distribution.

4.2. Bayesian estimation

Bayesian inference offers a versatile framework for parameter estimation by explicitly incorporating prior uncertainty. It updates beliefs about the parameters, expressed through prior distributions $\omega(\boldsymbol{\Theta})$,

using the observed data via the likelihood function $L(\underline{\mathbf{x}}|\Theta)$ to form the posterior distribution $\omega(\Theta|\underline{\mathbf{x}})$. This approach is particularly beneficial for complex models like the FEPW distribution, where it enables robust inference on intricate reliability metrics.

The posterior distribution is proportional to the product of the likelihood and the prior:

$$\omega(\Theta|\underline{\mathbf{x}}) \propto L(\underline{\mathbf{x}}|\Theta)\,\omega(\Theta). \tag{4.3}$$

The choice of prior distributions is crucial. Given that all parameters $\tau, \eta, \kappa, \varphi$ are strictly positive, independent Gamma distributions are often chosen as priors due to their flexibility and support on the positive real line [8, 9]. Accordingly, the prior distributions are specified as follows:

$$\omega(\Theta) = \omega_1(\tau)\omega_2(\eta)\omega_3(\kappa)\omega_4(\varphi),$$

where $\omega(\Theta_k) \propto \Theta_k^{c_k-1} e^{-d_k\Theta_k}$ for $\Theta_k \in \{\tau, \eta, \kappa, \varphi\}$, with shape $c_k > 0$ and rate $d_k > 0$ hyperparameters. These hyperparameters can be set to reflect vague prior information (e.g., $c_k = d_k \approx 0$ for a near-flat prior) or to incorporate expert knowledge. The resulting joint posterior distribution is:

$$\omega(\Theta|\underline{\mathbf{x}}) \propto \tau^{c_1-1}\eta^{c_2-1}\kappa^{c_3-1}\varphi^{c_4-1}\,\mathrm{e}^{-(d_1\tau+d_2\eta+d_3\kappa+d_4\varphi)}\,\mathrm{e}^{-\sum_{i=1}^{n}\left(\mathrm{e}^{(\tau x_i)^\eta}+(\kappa x_i)^\varphi\right)}\prod_{i=1}^{n} h(x_i;\Theta),$$

where $h(x_i;\Theta) = \left(\tau\eta(\tau x_i)^{\eta-1}\mathrm{e}^{(\tau\, x_i)^\eta} + \kappa\varphi(\kappa x_i)^{\varphi-1}\right)$.

The full conditional distributions of τ, η, κ, and φ are given as follows:

$$\omega(\tau|\eta,\kappa,\varphi,\underline{\mathbf{x}}) \propto \tau^{c_1-1}\mathrm{e}^{-(d_1\tau+\sum_{i=1}^{n}\mathrm{e}^{(\tau x_i)^\eta})}\prod_{i=1}^{n} h(x_i;\Theta),$$

$$\omega(\eta|\tau,\kappa,\varphi,\underline{\mathbf{x}}) \propto \eta^{c_2-1}\mathrm{e}^{-(d_2\eta+\sum_{i=1}^{n}\mathrm{e}^{(\tau x_i)^\eta})}\prod_{i=1}^{n} h(x_i;\Theta),$$

$$\omega(\kappa|\tau,\eta,\varphi,\underline{\mathbf{x}}) \propto \kappa^{c_3-1}\mathrm{e}^{-(d_3\kappa+\sum_{i=1}^{n}(\kappa x_i)^\varphi)}\prod_{i=1}^{n} h(x_i;\Theta),$$

$$\omega(\varphi|\tau,\eta,\kappa,\underline{\mathbf{x}}) \propto \varphi^{c_4-1}\mathrm{e}^{-(d_4\varphi+\sum_{i=1}^{n}(\kappa x_i)^\varphi)}\prod_{i=1}^{n} h(x_i;\Theta).$$

Under the squared error loss function, the Bayes estimator for a parameter θ_j is its posterior mean:

$$\hat{\Theta}_j^{\text{Bayes}} = \mathbb{E}[\Theta_j|\underline{\mathbf{x}}] = \int \Theta_j\,\omega(\boldsymbol{\Theta}|\underline{\mathbf{x}})\,d\boldsymbol{\Theta}.$$

4.3. Hamiltonian Monte Carlo with NUTS

Traditional Markov chain Monte Carlo (MCMC) methods, such as Metropolis–Hastings and Gibbs sampling, often exhibit inefficiencies in high-dimensional or correlated parameter spaces due to random-walk behavior, leading to slow convergence and high autocorrelation [16–18]. Hamiltonian Monte Carlo (HMC) addresses these issues by exploiting gradient information from the log-posterior

density to propose more informed states in the parameter space, thereby reducing the random-walk behavior typical of simpler MCMC algorithms and producing less autocorrelated samples [19].

The No-U-Turn Sampler (NUTS) is an adaptive extension of HMC that automatically tunes the trajectory length of the Hamiltonian simulation, eliminating the need for manual specification of this critical parameter [20]. By dynamically building candidate states and stopping when the simulated trajectory starts to reverse direction, NUTS enables efficient posterior exploration without requiring a fixed number of leapfrog steps. This adaptive feature makes NUTS more robust and practically convenient while preserving the efficiency advantages of HMC [20–22].

Developments have further extended HMC toward learned and adaptive variants, broadening its applicability in challenging Bayesian computation settings [23, 24]. In this study, the HMC–NUTS algorithm is implemented in Wolfram Mathematica. For each dataset, M parallel chains are run, each with N_T total iterations, of which N_B iterations are discarded as burn-in/adaptation. Convergence is assessed using the Gelman–Rubin statistic ($\hat{R}$) and the effective sample size (ESS).

Posterior samples after burn-in are pooled, and Bayes estimates for the scalar model parameters are approximated by

$$\hat{\Theta}_j \approx \frac{1}{N_{\mathrm{C}}(N_{\mathrm{T}} - N_{\mathrm{B}})} \sum_{i=1}^{N_{\mathrm{C}}} \sum_{l=N_B+1}^{N_T} \Theta_{i,l},$$

where N_C is the number of chains, N_T is the total number of iterations per chain, and N_B is the number of discarded burn-in iterations per chain. These posterior draws were also used to construct highest posterior density (HPD) credible intervals for parameter uncertainty quantification.

In the Bayesian analysis, posterior inference for nonlinear functionals was carried out by evaluating the quantity of interest at each posterior draw of the parameter vector rather than substituting posterior mean estimates directly into the functional form. In particular, for each retained posterior sample, the reliability and hazard functions were computed pointwise over the corresponding time grid, and the resulting posterior function values were then summarized at each time point. Accordingly, the fitted Bayesian curves reported in this study represent the posterior mean function with the associated 95% HPD intervals. This strategy provides a more faithful characterization of posterior uncertainty for nonlinear transformations and avoids the potential distortion that may arise from plug-in evaluation based solely on posterior mean parameter estimates.

The NUTS (Algorithm 1) was implemented within the Mathematica environment, leveraging its robust capabilities for this complex task. The symbolic computation engine ensured precise gradient evaluations, while high-precision numerical solvers like `NDSolve` performed the leapfrog integration. Built-in parallelization, through functions such as `ParallelTable`, enables the concurrent execution of multiple chains for improved sampling. Following the sampling phase, key diagnostic metrics, including the $\hat{R}$ and ESS, were computed using Mathematica's statistical functions to rigorously assess chain convergence and sampling efficiency. This integrated approach facilitated reproducible computation, facilitating accurate and scalable Bayesian inference for high-dimensional models. The implementation was further supported by comprehensive graphical representations to elucidate the characteristics of the posterior distribution and the convergence behavior of the chains.

Algorithm 1 No-U-Turn Sampler (NUTS) algorithm with dual averaging and diagnostics

Phase 1: Initialization
Require: Observed data $\mathbf{x}$, number of chains N_C, total iterations per chain N_T, burn-in iterations N_B, initial step size ϵ, target acceptance rate δ, maximum tree depth $J_{\max}$, and dual-averaging parameters (γ, t_0, κ).
for $c = 1$ to N_{C} **do**
    Initialize $\boldsymbol{\Theta}_c^{(0)} \sim$ Random starting point
end for

Phase 2: NUTS Sampling Loop
for $c = 1$ to N_{C} **do**
    for $t = 1$ to N_{T} **do**
        Sample momentum: $\mathbf{p} \sim \mathcal{N}(0, M)$
        Compute Hamiltonian: $H(\boldsymbol{\Theta}_c^{(t)}, \mathbf{p}) = -\log \omega(\boldsymbol{\Theta}_c^{(t)}|\underline{\mathbf{x}}) + \frac{1}{2}\mathbf{p}^T M\mathbf{p}$
        Sample slice variable: $u \sim \mathrm{Uniform}(0, \exp(-H(\boldsymbol{\Theta}_c^{(t)}, \mathbf{p})))$
        Build balanced binary tree via recursive leapfrog steps, stopping when U-turn condition is met or max depth reached
        Select next state $\boldsymbol{\Theta}_c^{(t+1)}$ from valid trajectory states
        if $t \leq N_{\mathrm{B}}$ **then** ▷ Burn-in phase
            Adapt step size ε using Dual Averaging targeting acceptance rate δ
        end if
    end for
end for

Phase 3: Post-Sampling Diagnostics
Combine samples: $\{\Theta_c^{(t)}\}$ for $c = 1, \ldots, N_C$ and $t = N_B + 1, \ldots, N_T$
Calculate $\hat{R}$ statistic ▷ Target: $\hat{R} < 1.01$
Calculate ESS ▷ Target: High ESS
Output: Posterior distributions, summary statistics, diagnostics

Return: Combined posterior samples $\{\Theta^{(i)}\}_{i=1}^{N_C \times (N_T - N_B)}$

5. Simulation results

In this section, I examine the finite-sample performance of the proposed estimators for the FEPW distribution using the MLE and Bayesian inference. The simulation framework evaluates estimator accuracy, bias, and stability across parameter settings and a range of sample sizes. The procedure used in the simulation study is summarized in Algorithm 2.

Algorithm 2 Simulation procedure for evaluating FEPW parameter estimators

Specify the true parameter vector $\boldsymbol{\psi}_0 = (\tau_0, \eta_0, \kappa_0, \varphi_0)$.
Select sample sizes $n \in \{30, 60, 120, 200, 300\}$.
Generate a random sample of size n from the FEPW distribution.
Estimate $\boldsymbol{\psi}$ using MLE by maximizing the log-likelihood function.
Estimate $\boldsymbol{\psi}$ under a Bayesian framework using Gamma priors and HMC–NUTS.
Repeat Steps 2–5 for $N = 1000$ Monte Carlo replications.
Compute Monte Carlo bias and MSE for each estimator.
Compare the results across estimation methods and sample sizes.

The simulation experiments were implemented in *R* via the *Stan* interface. For each Monte Carlo replication, the HMC–NUTS algorithm was run using $N_C = 4$ parallel chains, each with $N_T = 2000$ total iterations, of which $N_B = 1000$ iterations were discarded as warm-up. The sampler control settings were $\delta = 0.90$ (`adapt_delta`) and $J_{\max} = 12$ (`max_treedepth`). Convergence was monitored using $\hat{R}$, and only runs satisfying $\hat{R} < 1.01$ for all parameters were retained.

Tables 3 and 4 report the Monte Carlo bias and mean squared error (MSE) for each parameter under the MLE and Bayesian approaches, respectively, while Figure 6 provides graphical comparisons across sample sizes. The noteworthy patterns revealed by the analysis are as follows:

- **Consistency and efficiency:** The bias and MSE decrease steadily as the sample size increases from $n = 30$ to $n = 300$ under all parameter configurations. This behavior aligns with asymptotic theory and confirms that MLE and Bayesian estimators perform well for the FEPW distribution.
- **Small-sample performance:** Bayesian estimation demonstrates superior performance in small samples. In particular, when $n \in \{30, 60\}$, the Bayesian approach produces noticeably lower bias and MSE than MLE for shape parameter φ, which is more sensitive to sample variability. The introduction of Gamma priors helps stabilize the estimation process when data are limited.
- **Large-sample convergence:** As sample size increases to $n = 200$ and $n = 300$, both estimation methods converge to nearly identical results, exhibiting very small bias and MSE. These findings confirm that MLE becomes competitive with Bayesian inference once sufficient data are available, while Bayesian inference remains advantageous in small-sample settings.
- **Parameter-specific estimation patterns:** The estimation accuracy varies substantially across parameters. Scale parameter τ demonstrates high estimation precision under both methods, even in small-sample scenarios, as evidenced by consistently minimal bias and error measures. Conversely, estimation of shape parameter φ proves more challenging, particularly for MLE with limited data, where instability is most pronounced. This evident difficulty can be attributed to the flatness of the likelihood surface with respect to φ. In complex distributions like FEPW, shape parameters often govern the tail behavior, which requires sufficient data points in the extremes for accurate estimation. In small samples ($n \leq 60$), the lack of tail information leads to high variance and instability in MLE. This emphasizes the advantage of the Bayesian approach, where incorporating informative Gamma priors regularizes the estimation space, preventing estimates from diverging due to sample variability.

Overall, the simulation study demonstrates that the proposed estimation procedures yield accurate, stable, and robust estimates for the FEPW distribution under a wide range of configurations.

Table 3. Monte Carlo bias and MSE for the MLE estimates of the FEPW parameters under four true parameter configurations and sample sizes $n \in \{30, 60, 120, 200, 300\}$. Values smaller than 10^{-6} are reported as 0.0000.

n	Bias				MSE			
	$\hat{\tau}$	$\hat{\eta}$	$\hat{\kappa}$	$\hat{\varphi}$	$\hat{\tau}$	$\hat{\eta}$	$\hat{\kappa}$	$\hat{\varphi}$
$\hat{\tau} = 0.01$, $\hat{\eta} = 0.5$, $\hat{\kappa} = 0.02$, $\hat{\varphi} = 6$								
30	0.001128	0.033190	0.000035	0.597000	0.000027	0.020310	0.000002	11.18000
60	0.000633	0.019330	-0.000019	-0.258600	0.000014	0.009438	0.000000	2.090000
120	0.000350	0.009384	-0.000045	0.105300	0.000007	0.004748	0.000000	0.824800
200	0.000239	0.005760	-0.000021	0.074616	0.000005	0.003039	0.000000	0.545000
300	0.000206	0.005004	-0.000034	0.075044	0.000004	0.002132	0.000000	0.506800
$\hat{\tau} = 0.2$, $\hat{\eta} = 4$, $\hat{\kappa} = 0.05$, $\hat{\varphi} = 0.5$								
30	0.000792	1.340287	0.032860	0.088345	0.000076	25.31000	0.005547	0.069880
60	0.000433	0.440306	0.018165	0.044312	0.000038	1.420000	0.002621	0.026010
120	0.000201	0.145485	0.006736	0.012231	0.000018	0.388700	0.001072	0.014100
200	0.000304	0.086459	0.003107	0.002202	0.000011	0.214000	0.000702	0.006148
300	0.000152	0.065257	0.001693	-0.000681	0.000009	0.140600	0.000472	0.004078
$\hat{\tau} = 0.08$, $\hat{\eta} = 3.4$, $\hat{\kappa} = 0.05$, $\hat{\varphi} = 0.7$								
30	0.000279	2.456191	0.013221	0.096229	0.000026	65.56000	0.001467	0.088130
60	0.000058	0.814700	0.008148	0.059190	0.000015	4.779000	0.000902	0.045220
120	-0.000002	0.268900	0.003264	0.021850	0.000007	0.726800	0.000456	0.018910
200	0.000029	0.179500	0.002217	0.014460	0.000004	0.347800	0.000303	0.011390
300	-0.000011	0.132800	0.001648	0.009023	0.000003	0.218300	0.000020	0.006909
$\hat{\tau} = 0.001$, $\hat{\eta} = 0.28$, $\hat{\kappa} = 0.03$, $\hat{\varphi} = 5.6$								
30	0.001905	0.037666	-0.000117	0.050156	0.000012	0.009147	0.000002	0.439400
60	0.001261	0.024670	0.000029	0.087380	0.000477	0.003982	0.000001	0.477300
120	0.000864	0.022780	0.000011	0.044540	0.000002	0.002463	0.000000	0.429800
200	0.000741	0.019200	-0.000023	-0.050210	0.000001	0.001322	0.000000	0.424100
300	0.000621	0.021330	-0.000009	-0.031350	0.000000	0.001130	0.000000	0.447800

Table 4. Monte Carlo bias and MSE for the Bayesian HMC–NUTS estimates of the FEPW parameters under four true parameter configurations and sample sizes $n \in \{30, 60, 120, 200, 300\}$. Values smaller than 10^{-6} are reported as 0.0000.

n	Bias				MSE			
	$\hat{\tau}$	$\hat{\eta}$	$\hat{\kappa}$	$\hat{\varphi}$	$\hat{\tau}$	$\hat{\eta}$	$\hat{\kappa}$	$\hat{\varphi}$
$\hat{\tau} = 0.01$, $\hat{\eta} = 0.5$, $\hat{\kappa} = 0.02$, $\hat{\varphi} = 6$								
30	0.001324	0.132187	-0.005843	-0.782523	0.000102	1.417348	0.000143	3.774283
60	-0.001486	-0.027093	-0.000129	-0.123161	0.000022	0.014300	0.000017	2.900000
120	-0.000582	-0.010979	0.000207	-0.020868	0.000008	0.004536	0.000000	1.391000
200	-0.000355	-0.006398	0.000133	0.013862	0.000006	0.002987	0.000000	0.849700
300	-0.000234	-0.004616	0.000072	0.029285	0.000004	0.001861	0.000000	0.523900
$\hat{\tau} = 0.2$, $\hat{\eta} = 4$, $\hat{\kappa} = 0.05$, $\hat{\varphi} = 0.5$								
30	-0.001238	1.709642	0.028550	0.444006	0.000188	9.906689	0.004309	9.973410
60	-0.000561	0.720961	0.019967	0.092794	0.000040	2.057000	0.002572	2.883000
120	-0.000284	0.258881	0.008058	0.001988	0.000018	0.452100	0.001071	0.011440
200	-0.000003	0.148700	0.004278	-0.001893	0.000011	0.231900	0.000667	0.006179
300	0.000045	0.098975	0.002147	-0.004616	0.000008	0.146200	0.000426	0.003987
$\hat{\tau} = 0.08$, $\hat{\eta} = 3.4$, $\hat{\kappa} = 0.05$, $\hat{\varphi} = 0.7$								
30	0.008195	-1.222730	-0.039020	3.839967	0.000127	2.364000	0.001797	25.63000
60	0.004861	-0.532630	-0.022845	1.562126	0.000065	1.478000	0.000977	1.123000
120	0.000917	-0.094458	-0.007053	0.007275	0.000009	0.346000	0.000345	0.330200
200	0.000539	-0.032277	-0.003422	-0.016563	0.000004	0.234000	0.000254	0.009471
300	0.000308	-0.003745	-0.002049	-0.009299	0.000003	0.169100	0.000173	0.006427
$\hat{\tau} = 0.001$, $\hat{\eta} = 0.28$, $\hat{\kappa} = 0.03$, $\hat{\varphi} = 5.6$								
30	-0.000006	-0.065060	0.001971	-2.652000	0.000006	0.022470	0.000013	7.045000
60	-0.000317	-0.048042	0.001915	-2.418967	0.000000	0.005977	0.000005	5.867000
120	-0.000477	-0.042448	0.001503	-2.028786	0.000000	0.003744	0.000003	4.143000
200	-0.000481	-0.036633	0.001189	-1.639567	0.000000	0.002550	0.000002	2.723000
300	-0.000448	-0.031342	0.000914	-1.313406	0.000000	0.001835	0.000001	1.763000

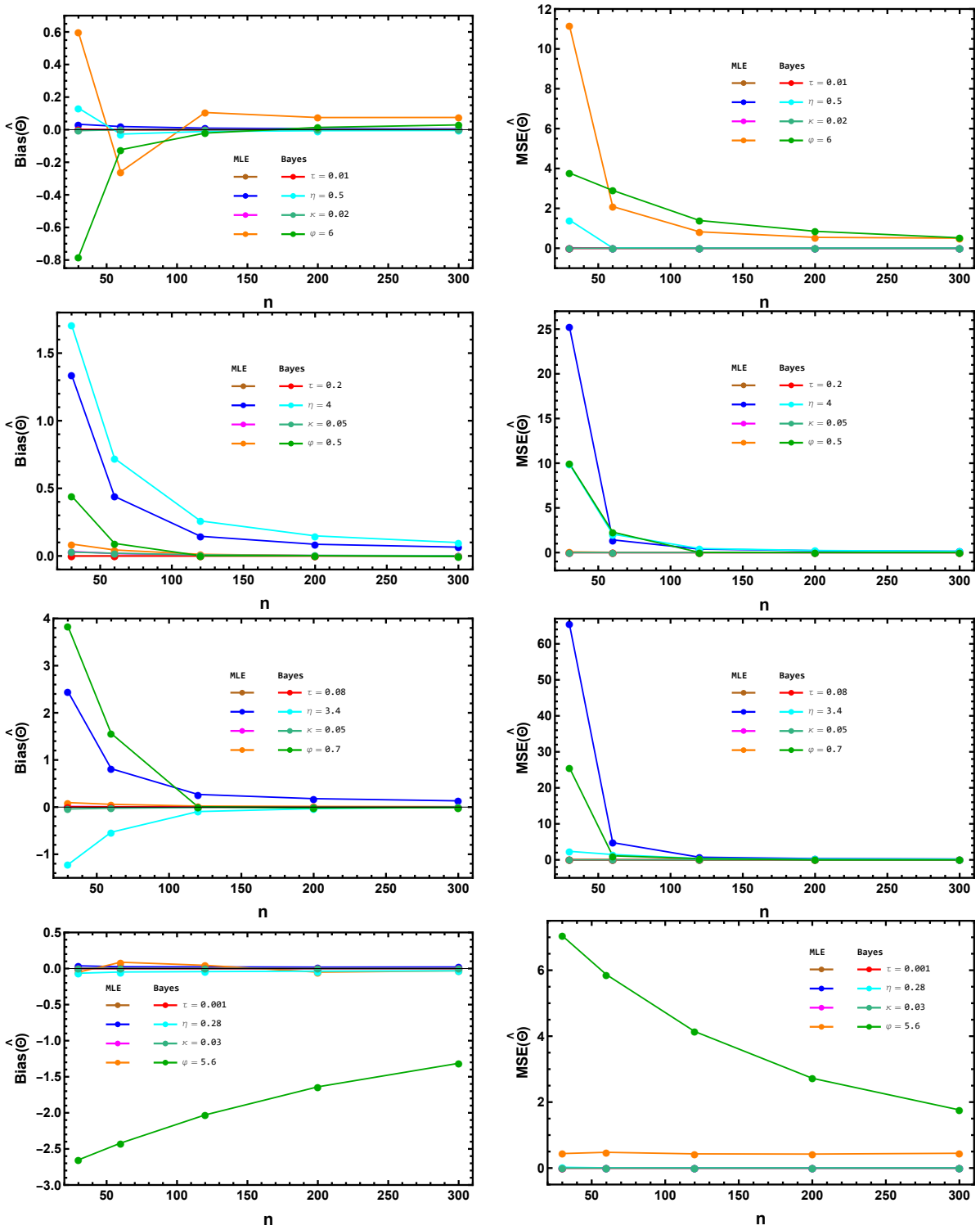

Figure 6. Comparison of bias and MSE for the MLE and Bayesian estimators of the FEPW parameters under four parameter configurations.

6. Real data applications

In this section, I illustrate the practical utility and flexibility of the proposed FEPW distribution by analyzing three distinct real-world datasets. The primary objective is to evaluate the goodness-of-fit of the FEPW model and benchmark its performance against the competitive Weibull extensions listed in Table 5. To ensure a robust analysis, I adopt the Bayesian estimation framework detailed in Section 4.

For the real-data applications, the Mathematica implementation of HMC–NUTS used $N_C = 4$ parallel chains, each with $N_T = 4000$ total iterations, including $N_B = 1500$ burn-in/adaptation iterations. The initial step size ϵ was selected automatically using a heuristic search procedure (`FindReasonableEps`) and subsequently adapted during burn-in via dual averaging. The target acceptance rate was fixed at $\delta = 0.9$, and the dual-averaging parameters were set to $\gamma = 0.05$, $t_0 = 10$, and $\kappa = 0.75$. The maximum tree depth was fixed at $J_{\max} = 20$. Posterior inference was based on the retained post-burn-in samples from all chains. Convergence and sampling efficiency were evaluated using trace plots, posterior density plots, $\hat{R}$, and ESS.

Table 5. List of competing lifetime distributions with their corresponding CDFs and parameter spaces.

Distribution	Ref.	CDF	Parameter space
MWE	[25]	$1 - e^{\tau\eta\left(1-e^{\left(\frac{x}{\tau}\right)^{\kappa}}\right)}$	$\tau, \eta, \kappa > 0$
MW	[26]	$1 - e^{-\tau x^{\eta} e^{\kappa x}}$	$\tau, \eta, \kappa > 0$
NMW	[27]	$1 - e^{1-e^{\tau x^{\eta} e^{\kappa x}}}$	$\tau, \eta, \kappa > 0$
AW	[10]	$1 - e^{-\kappa x^{\varphi} - \tau x^{\eta}}$	$\tau, \eta, \kappa, \varphi > 0$
EMWE	[28]	$\left(1 - e^{\tau\varphi\left(1-e^{\left(\frac{x}{\tau}\right)^{\eta}}\right)}\right)^{\kappa}$	$\tau, \eta, \kappa, \varphi > 0$
ACW	[13]	$1 - e^{\varphi\left(1-e^{x^{\kappa}}\right)-(\tau x)^{\eta}}$	$\tau, \eta, \kappa, \varphi > 0$
WMW	[11]	$1 - e^{-\kappa e^{\xi x} x^{\varphi} - \tau x^{\eta}}$	$\tau, \eta, \kappa, \varphi, \xi > 0$
GExtEW	[29]	$\left(1 - e^{-(\tau x^{\eta} + \kappa x)^{\varphi}}\right)^{\xi}$	$\tau, \eta, \kappa, \varphi, \xi > 0$
MWC	[30]	$1 - e^{\varphi\left(1-e^{x^{\xi}}\right)-\tau x^{\eta} e^{\kappa x}}$	$\tau, \eta, \kappa, \varphi, \xi > 0$

To facilitate a rigorous comparison between the FEPW distribution and the competing models, I utilized a comprehensive set of statistical criteria. I computed the negative log-likelihood ($-\ell$) and four information-theoretic criteria: the Akaike Information Criterion ($\mathcal{I}_A$), Corrected AIC ($\mathcal{I}_{Ac}$), Bayesian Information Criterion ($\mathcal{I}_B$), and Hannan–Quinn Information Criterion ($\mathcal{I}_{HQ}$). Furthermore, to assess the distance between the empirical and theoretical distributions, I employed the Kolmogorov distance statistic (D_n), the Cramér–von Mises statistic (W^2), and the Anderson–Darling statistic (A^2). In my comparative analysis, models yielding the lowest values for these metrics were considered the best fit for the data. To further visualize the performance hierarchy, I generated ranking plots for these statistics. Finally, the adequacy of the proposed model was visually assessed by superimposing the estimated reliability, and HRFs over the empirical data. All statistical computations and graphical representations were executed using the Wolfram Mathematica software platform.

6.1. Application 1: Voltage endurance life of electrodes (VETEs)

The first dataset, denoted by VETEs, consists of the voltage endurance lifetimes (in hours) of $n = 58$ epoxy resin insulation electrodes [9, 31]. This dataset is a well-known benchmark in reliability engineering and is frequently used to assess the flexibility of lifetime distributions in modeling failure data with complex hazard-rate structures.

Prior to model fitting, I examined the qualitative behavior of the failure rate using the scaled Total Time on Test (TTT) transform plot shown in Figure 7. The empirical TTT curve exhibits an initial convex segment near the origin, followed by a concave portion, and finally a convex trend toward the tail. This curvature pattern suggests that the underlying hazard rate may exhibit a bathtub-shaped or modified unimodal form. Consequently, fitting a flexible distribution such as the FEPW model is appropriate for representing these phases.

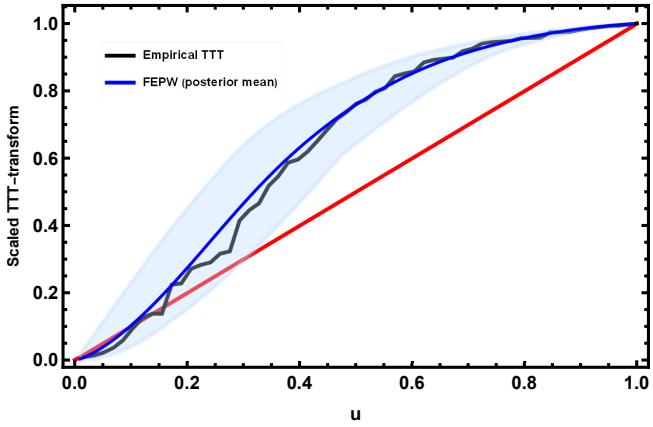

Figure 7. Empirical scaled TTT transform for the VETEs dataset with the fitted FEPW posterior mean curve and its 95% HPD uncertainty band.

The maximum likelihood estimates of the parameters for the FEPW distribution and the competing models are reported in Table 6. To assess model adequacy more formally, Table 7 presents the goodness-of-fit statistics and information-theoretic criteria. The results indicate that the proposed FEPW distribution provides the strongest overall performance for the VETEs dataset. In particular, the FEPW model attains the smallest values of the principal information criteria, including the negative log-likelihood ($-\ell = 350.093$) and $\mathcal{I}_A = 708.186$.

To provide additional numerical evidence for parameter identifiability and the stability of the likelihood-based estimates, I also report the FIM evaluated at the MLEs for the VETEs dataset:

$$\mathbf{I}(\widehat{\boldsymbol{\Theta}}) = \begin{bmatrix} 3.60233 \times 10^{-7} & 0.0000637151 & -6.06456 \times 10^{-8} & 0.00049502 \\ 0.0000637151 & 0.0205009 & -0.00001067 & 0.082232 \\ -6.06456 \times 10^{-8} & -0.00001067 & 2.52372 \times 10^{-8} & -0.000157226 \\ 0.00049502 & 0.082232 & -0.000157226 & 2.41817 \end{bmatrix}.$$

With respect to the distance-based goodness-of-fit measures, the FEPW distribution also performed very strongly, attaining the smallest values of $D_n = 0.0428$, $W^2 = 0.07816$, and $A^2 = 0.00913$. Since smaller values of these statistics indicate closer agreement between the empirical data and the fitted model, these results further support the adequacy of the FEPW distribution for the VETEs dataset. The

overall comparative ranking is summarized in Figure 8, where the FEPW model consistently achieves the top rank across the considered criteria.

Table 6. Maximum likelihood estimates of the parameters for the FEPW distribution and competing models fitted to the VETEs dataset.

Distribution	$\hat{\tau}$	$\hat{\eta}$	$\hat{\kappa}$	$\hat{\varphi}$	$\hat{\xi}$
MWE	86.902	1.43051×10^{-3}	0.74902		
MW	0.01598	0.48172	5.73717×10^{-3}		
NMW	0.01557	0.5152	3.52531×10^{-3}		
FEPW	1.59596×10^{-3}	0.69339	2.83718×10^{-3}	6.14582	
AW	2.13036×10^{-10}	3.84687	0.0133	0.67248	
EMWE	217.879	1.96542	0.33407	3.63949×10^{-4}	
ACW	2.79003×10^{-3}	6.49762	0.25124	0.01359	
WMW	0.01178	0.70927	2.87574×10^{-4}	0.61986	0.01329
GExtEW	1.17691	4.21506×10^{-3}	1.89723×10^{-4}	8.04426	181.349
MWC	6.10126×10^{-4}	0.31223	0.0157	0.01378	0.24675

Table 7. Goodness-of-fit statistics and information-theoretic criteria for the FEPW distribution and competing models fitted to the VETEs dataset. Superscripts denote model ranks from 1 (best) to 10 (worst).

Distribution	$-\ell$	$\mathcal{I}_A$	$\mathcal{I}_{Ac}$	$\mathcal{I}_B$	$\mathcal{I}_{HQ}$	D_n (p value)	W^2 (p-value)	A^2 (p value)
MWE	355.416^{9}	716.831^{9}	717.276^{9}	723.013^{7}	719.239^{9}	$0.10467\ (0.5488)^{9}$	$1.17142\ (0.27848)^{9}$	$0.16675\ (0.34304)^{9}$
MW	353.785^{8}	715.571^{8}	716.325^{8}	723.812^{8}	718.781^{8}	$0.09142\ (0.71751)^{8}$	$0.6393\ (0.61093)^{8}$	$0.10635\ (0.55609)^{8}$
NMW	352.065^{7}	714.129^{7}	715.283^{7}	724.431^{9}	718.142^{7}	$0.0837\ (0.81124)^{7}$	$0.3963\ (0.85185)^{7}$	$0.06608\ (0.77777)^{7}$
FEPW	350.093^{1}	708.186^{1}	$708.94^{\ 1}$	716.427^{1}	711.396^{1}	$0.0428\ (0.99993)^{1}$	$0.07816\ (0.99999)^{1}$	$0.00913\ (0.99999)^{1}$
AW	351.448^{6}	710.896^{5}	711.651^{5}	719.138^{4}	714.106^{4}	$0.0712\ (0.93037)^{6}$	$0.25089\ (0.96984)^{6}$	$0.0429\ (0.91943)^{6}$
EMWE	350.622^{3}	709.245^{2}	709.999^{2}	717.486^{2}	712.455^{2}	$0.05287\ (0.99691)^{5}$	$0.13543\ (0.99941)^{5}$	$0.01883\ (0.99815)^{5}$
ACW	$350.94^{\ 4}$	709.879^{3}	710.634^{3}	718.121^{3}	$713.09^{\ 3}$	$0.04989\ (0.99872)^{3}$	$0.10458\ (0.99996)^{3}$	$0.01157\ (0.99997)^{3}$
WMW	350.169^{2}	710.337^{4}	711.491^{4}	$720.64^{\ 5}$	$714.35^{\ 5}$	$0.04358\ (0.9999)^{2}$	$0.08444\ (0.99998)^{2}$	$0.0103\ (0.99998)^{2}$
GExtEW	359.518^{10}	729.037^{10}	730.191^{10}	739.339^{10}	$733.05^{\ 10}$	$0.12909\ (0.28858)^{10}$	$1.3301\ (0.22274)^{10}$	$0.22459\ (0.22472)^{10}$
MWC	351.219^{5}	712.591^{6}	713.591^{6}	$722.74^{\ 6}$	$716.45^{\ 6}$	$0.0528\ (0.99697)^{4}$	$0.12809\ (0.99965)^{4}$	$0.01499\ (0.99968)^{4}$

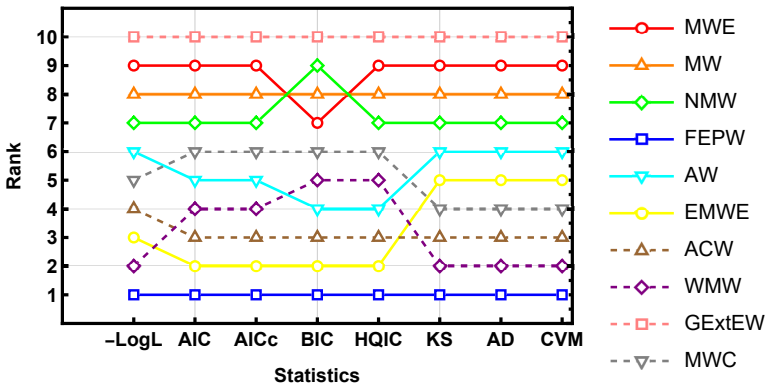

Figure 8. Comparative ranking plot of the fitted distributions across eight goodness-of-fit criteria for the VETEs dataset.

To complement the frequentist analysis, Bayesian estimation was carried out using the HMC–NUTS algorithm. Table 8 reports the posterior means, 95% CIs, 95% HPD intervals, and convergence diagnostics. The convergence behavior is satisfactory, with $\hat{R}$ values very close to 1, and ESS values indicating acceptable sampling efficiency.

To further assess the robustness of the Mathematica-based HMC–NUTS implementation, a sensitivity analysis with respect to the target acceptance rate was conducted for this application. The posterior summaries change only marginally across the examines settings, while the diagnostic performance remains most favorable at $\delta = 0.90$, supporting the stability of the Bayesian inference under moderate tuning changes.

Table 8. Maximum likelihood and Bayesian posterior estimates for the FEPW parameters under the VETEs dataset with 95% confidence intervals, 95% HPD intervals, and convergence diagnostics ($\hat{R}$, ESS).

Parameter	MLEs	95% CI	Bayes	95% HPD	$\hat{R}$	ESS
$\hat{\tau}$	0.00159	[0.00042, 0.00277]	0.00155	[0.00069, 0.00252]	1.00034	447
$\hat{\eta}$	0.69339	[0.41276, 0.97402]	0.68753	[0.46696, 0.95198]	1.00018	762
$\hat{\kappa}$	0.00284	[0.00253, 0.00315]	0.00283	[0.00251, 0.00319]	0.99994	467
$\hat{\varphi}$	6.14582	[3.09799, 9.19365]	5.86373	[3.56074, 8.94679]	1.00153	494

Visual inspection of the diagnostic plots in Figure 9 provides further support for satisfactory convergence of the HMC–NUTS sampler. The trace plots in Figure 9(a) display stable "fuzzy caterpillar" patterns, indicating adequate mixing of the four chains. The posterior density plots in Figure 9(b) are smooth and unimodal, while the box plots in Figure 9(c) show broadly consistent parameter distributions across chains, suggesting that the burn-in phase is adequate and that the posterior summaries are stable.

Furthermore, Figure 10 provides a joint view of the posterior distribution through a pairwise scatter plot matrix. The diagonal panels display the marginal posterior densities of the parameters, which appear unimodal and reasonably regular. The off-diagonal panels reveal the pairwise dependence structure among the parameters. For example, a positive correlation is observed between τ and η (correlation coefficient ≈ 0.639), whereas τ and κ exhibit a negative correlation (≈ -0.553). Despite these posterior dependencies, the HMC–NUTS sampler appears to explore the posterior distribution effectively, as also supported by the convergence diagnostics in Figure 9.

The goodness-of-fit is further illustrated graphically in Figure 11. The estimated RF of the FEPW distribution (Figure 11(a), solid blue line), with its associated 95% HPD uncertainty band (shaded region), follows the empirical survival curve closely and shows closer agreement than several competing models, particularly in the tail region. Moreover, the estimated HRF in Figure 11(c), with its corresponding 95% HPD uncertainty band (shaded region), successfully reproduces the bathtub-shaped failure behavior suggested by the TTT plot. A comparison of Figure 11(c) and (d) further indicates that the FEPW distribution provides a more realistic representation of the late-stage wear-out behavior than competing models such as MWE and ACW.

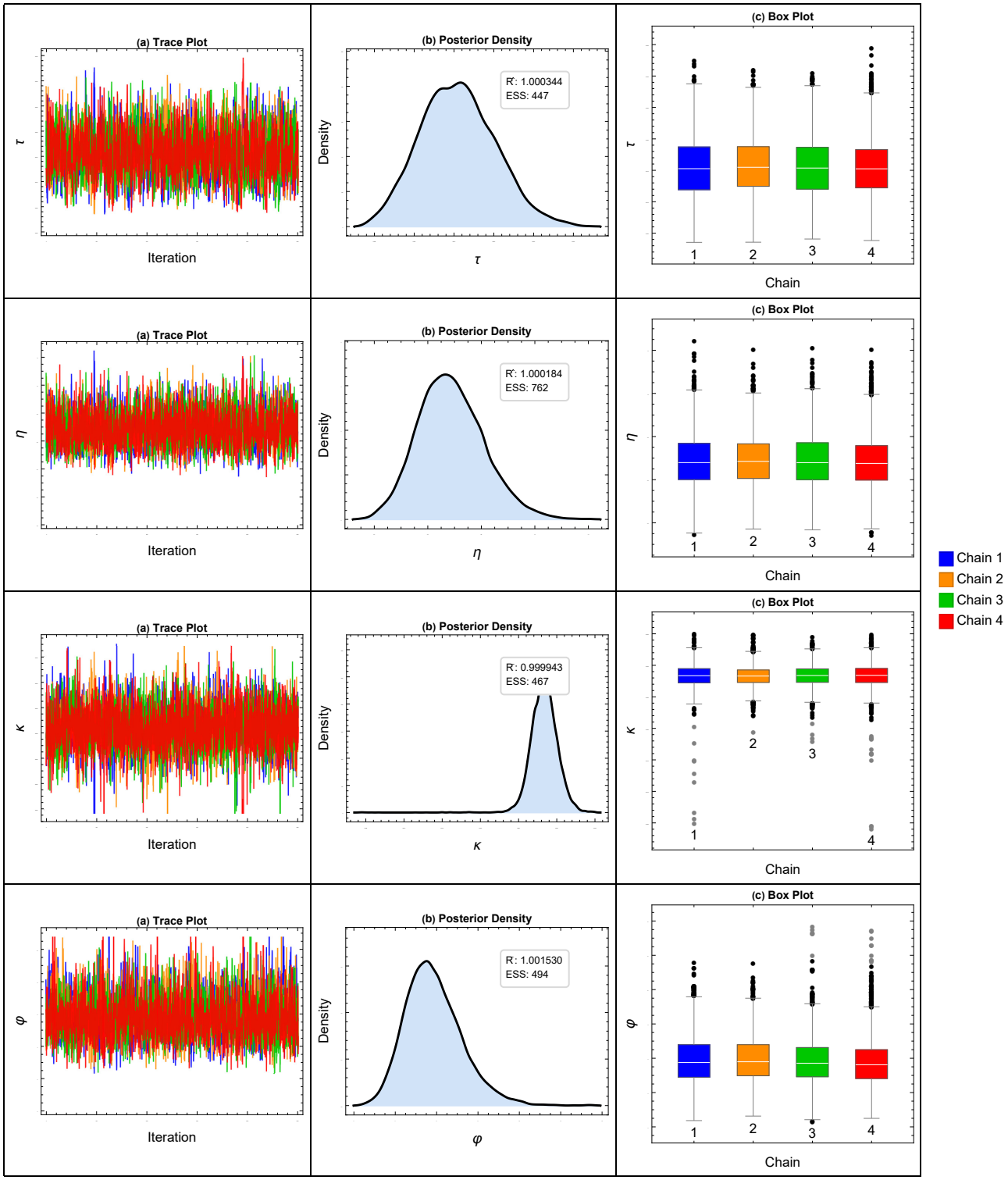

Figure 9. MCMC convergence diagnostics for the FEPW parameters under the VETEs dataset using the HMC–NUTS algorithm: (a) Trace plots, (b) marginal posterior density estimates, and (c) box plots across chains.

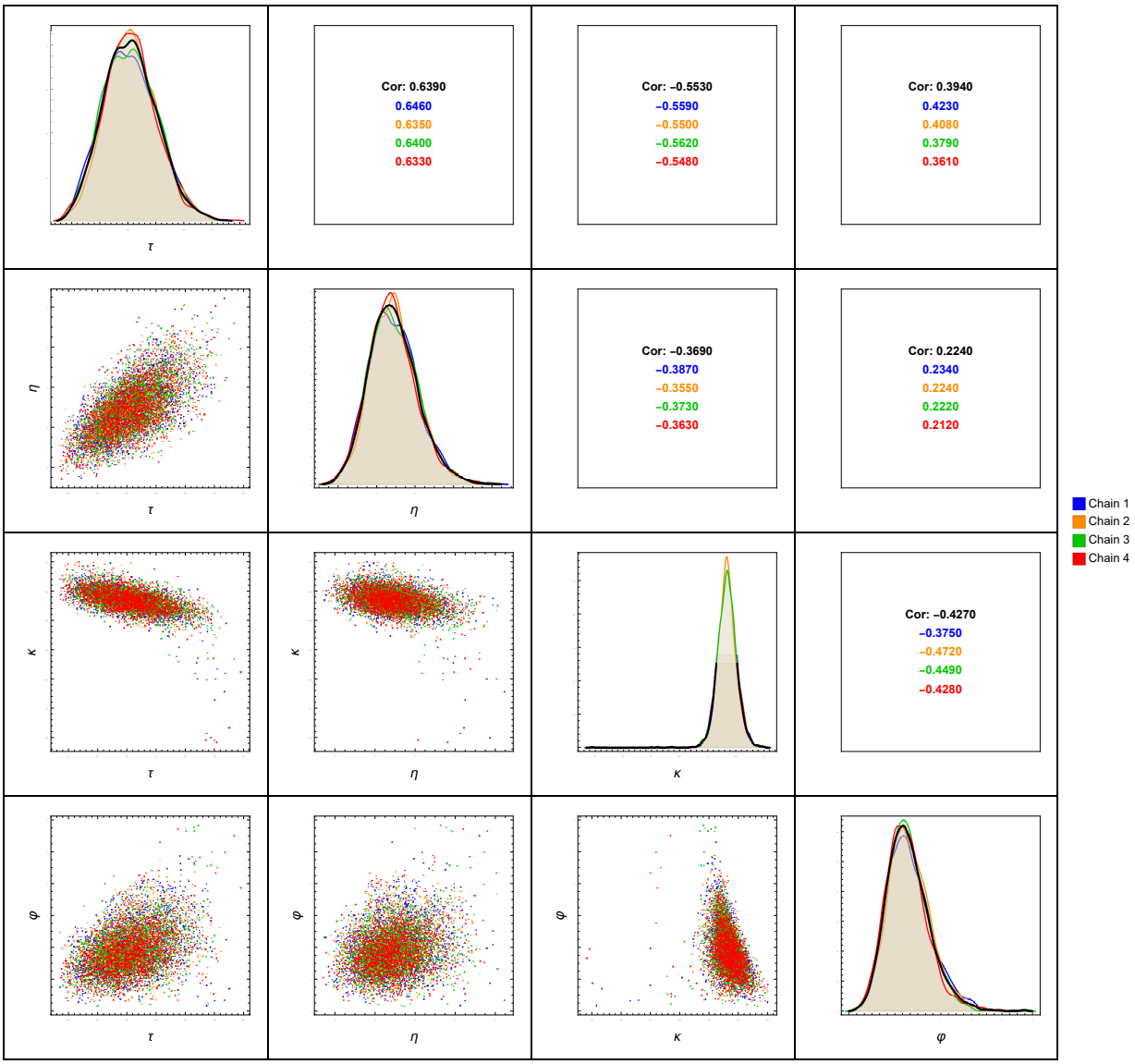

Figure 10. Pairwise scatter plot matrix of the FEPW posterior samples for the VETEs dataset, showing marginal posterior densities along the diagonal and pairwise dependence structures in the off-diagonal panels.

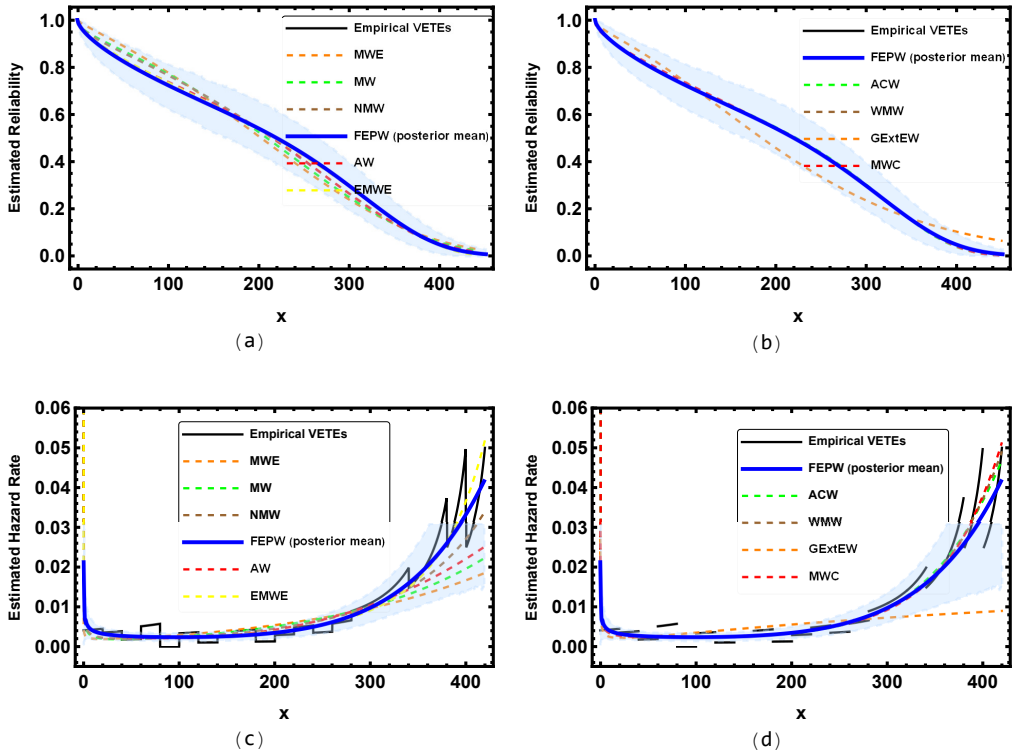

Figure 11. Graphical goodness-of-fit assessment for the VETEs dataset: (a) and (b) fitted reliability functions, and (c) and (d) estimated hazard rate functions for the FEPW model (posterior mean with 95% HPD band) and competing distributions.

6.2. Application 2: Aarset data

The second application was based on the Aarset dataset [32], which is a classical benchmark in reliability analysis and is well known for exhibiting non-monotone failure-rate behavior. Owing to its characteristic lifetime pattern, this dataset is frequently used to assess the ability of flexible lifetime distributions to model bathtub-shaped hazards.

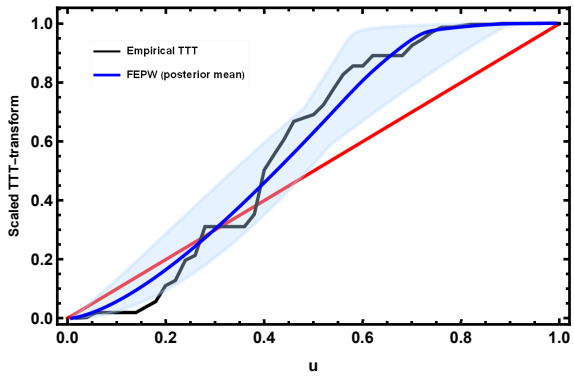

Figure 12. Empirical scaled TTT transform for the Aarset dataset with the fitted FEPW posterior mean curve and its 95% HPD uncertainty band.

Prior to formal model fitting, the qualitative behavior of the hazard rate was examined using the scaled Total Time on Test (TTT) transform shown in Figure 12. The empirical TTT curve exhibits an initial convex segment, followed by a concave portion, and finally a convex trend toward the tail. This curvature pattern suggests that the underlying hazard rate may possess a bathtub-shaped form. The fitted FEPW posterior mean curve with its 95% HPD uncertainty band follows the empirical TTT pattern reasonably well. Motivated by this qualitative evidence, Table 9 reports the maximum likelihood estimates of the FEPW distribution and the competing models.

Table 9. Maximum likelihood estimates of the parameters for the FEPW distribution and competing models fitted to the Aarset dataset.

Distribution	$\hat{\tau}$	$\hat{\eta}$	$\hat{\kappa}$	$\hat{\varphi}$	$\hat{\xi}$
MWE	13.7464	8.75964×10^{-3}	0.5877		
MW	0.0624	0.3548	0.02332		
NMW	0.06074	0.34329	0.01724		
FEPW	8.91614×10^{-3}	0.60515	0.01177	85.2192	
AW	6.98059×10^{-10}	4.85403	0.08115	0.44178	
EMWE	45.9876	3.37447	0.11072	5.79451×10^{-6}	
ACW	0.01177	86.8766	0.28443	0.04053	
WMW	0.04277	0.72599	1.56607×10^{-11}	0.71273	0.25903
GExtEW	0.74166	0.03498	1.53048×10^{-3}	69.7554	0.12343
MWC	1.3173×10^{-16}	1.12533	0.37367	0.03907	0.29102

To compare the fitted models more formally, Table 10 presents the goodness-of-fit statistics and information-theoretic criteria. The results indicate that the proposed FEPW model provides one of the strongest overall fits to the Aarset dataset. In particular, it achieves highly competitive values under the major likelihood-based and information-theoretic criteria, supporting its adequacy for modeling this dataset.

Bayesian estimation was then performed using the HMC–NUTS algorithm. Table 10 reports the posterior means, 95% CIs, 95% HPD intervals, and convergence diagnostics for the FEPW parameters. The diagnostic results are satisfactory, with $\hat{R}$ values very close to 1 and ESS values indicating acceptable sampling efficiency. The overall comparative ranking of the fitted models across the eight goodness-of-fit criteria is summarized in Figure 13.

Table 10. Goodness-of-fit statistics and information-theoretic criteria for the FEPW distribution and competing models fitted to the Aarset dataset. Superscripts denote model ranks from 1 (best) to 10 (worst).

Distribution	$-\ell$	$\mathcal{I}_A$	$\mathcal{I}_{Ac}$	$\mathcal{I}_B$	$\mathcal{I}_{HQ}$	D_n (p value)	W^2 (p-value)	A^2 (p value)
MWE	231.647^{10}	469.293^{10}	469.815^{10}	475.029^{10}	471.477^{10}	$0.15923\,(0.15839)^{10}$	$2.84913\,(0.03287)^{10}$	$0.37324\,(0.08478)^{10}$
MW	227.155^{9}	462.31^{9}	463.199^{9}	469.959^{9}	465.223^{9}	$0.13373\,(0.33295)^{7}$	$1.80557\,(0.11801)^{9}$	$0.26385\,(0.17156)^{9}$
NMW	224.301^{8}	458.602^{8}	459.966^{8}	468.162^{8}	462.242^{8}	$0.13851\,(0.29276)^{8}$	$1.78619\,(0.12099)^{8}$	$0.25158\,(0.18644)^{8}$
FEPW	204.906^{1}	417.812^{1}	418.701^{1}	425.46^{1}	420.725^{1}	$0.10063\,(0.69195)^{4}$	$0.58884\,(0.65776)^{2}$	$0.09128\,(0.63129)^{3}$
AW	220.629^{6}	449.259^{6}	450.148^{6}	456.907^{6}	452.171^{6}	$0.11467\,(0.5266)^{5}$	$1.04065\,(0.33626)^{6}$	$0.14102\,(0.41928)^{6}$
EMWE	212.837^{5}	433.673^{4}	434.562^{4}	441.321^{4}	436.585^{4}	$0.12219\,(0.44421)^{6}$	$0.88745\,(0.42149)^{5}$	$0.11225\,(0.52971)^{4}$
ACW	205.008^{2}	418.016^{2}	418.905^{2}	425.665^{2}	420.929^{2}	$0.08095\,(0.89859)^{1}$	$0.46366\,(0.78329)^{1}$	$0.06694\,(0.77273)^{1}$
WMW	212.156^{4}	434.312^{5}	435.676^{5}	443.872^{5}	437.952^{5}	$0.09813\,(0.72137)^{3}$	$0.84976\,(0.44588)^{3}$	$0.08604\,(0.65972)^{2}$
GExtEW	220.875^{7}	451.751^{7}	453.114^{7}	461.311^{7}	455.391^{7}	$0.15514\,(0.18007)^{9}$	$1.68061\,(0.13884)^{7}$	$0.22615\,(0.22229)^{7}$
MWC	209.66^{3}	429.321^{3}	430.684^{3}	438.881^{3}	432.961^{3}	$0.09651\,(0.74029)^{2}$	$0.85918\,(0.43965)^{4}$	$0.12534\,(0.47566)^{5}$

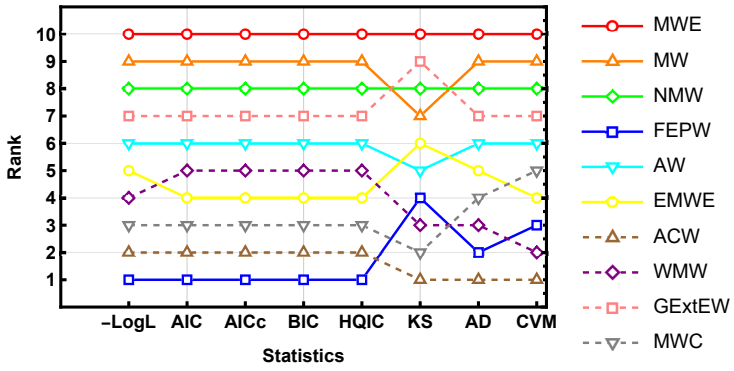

Figure 13. Comparative ranking plot of the fitted distributions across eight goodness-of-fit criteria for the Aarset dataset.

Table 11 reports the posterior means, 95% CIs, 95% HPD intervals, and convergence diagnostics for the FEPW parameters under the Aarset dataset. The convergence behavior is satisfactory, with $\hat{R}$ values very close to 1 and ESS values indicating acceptable sampling efficiency. Figure 14 provides the MCMC convergence diagnostics. The trace plots in Figure 14(a) display stable "fuzzy caterpillar" patterns, suggesting adequate mixing of the four chains. The posterior density plots in Figure 14(b) are smooth and unimodal, while the box plots in Figure 14(c) show broadly consistent posterior distributions across chains. Together, these diagnostics indicate that the burn-in phase is adequate and that the posterior summaries are stable.

Further insight into the dependence structure of the posterior samples is provided by the pairwise scatter plot matrix in Figure 15. The diagonal panels display the marginal posterior densities, which appear unimodal and reasonably regular, whereas the off-diagonal panels illustrate the pairwise dependence relationships among the parameters. Although some posterior dependence is present, the overall structure remains well behaved and is consistent with the satisfactory convergence diagnostics reported above.

The fitted reliability and HRFs are displayed in Figure 16. The FEPW distribution (solid blue line) with its associated 95% HPD uncertainty band (shaded region) provides a reasonable fit to the empirical reliability and hazard patterns. In particular, Figure 16(c) shows that the fitted hazard function captures the main bathtub-shaped behavior of the empirical hazard rate, especially in the early-failure and late wear-out phases. Compared with several competing models, the FEPW distribution offers a more plausible representation of the overall hazard-rate structure for the Aarset dataset.

Table 11. Maximum likelihood and Bayesian posterior estimates for the FEPW parameters under the Aarset dataset, together with 95% confidence intervals, 95% HPD intervals, and convergence diagnostics ($\hat{R}$, ESS).

Parameter	MLEs	95% CI	Bayes	95% HPD	$\hat{R}$	ESS
$\hat{\tau}$	0.00892	[0.00525, 0.01258]	0.00863	[0.00533, 0.01223]	1.00076	484
$\hat{\eta}$	0.60515	[0.60149, 0.79346]	0.59133	[0.30842, 0.78781]	1.00050	687
$\hat{\kappa}$	0.01177	[0.01167, 0.01187]	0.01177	[0.01168, 0.01187]	0.99990	1259
$\hat{\varphi}$	85.2192	[38.1651, 132.273]	80.812	[45.7204, 126.081]	1.00114	175

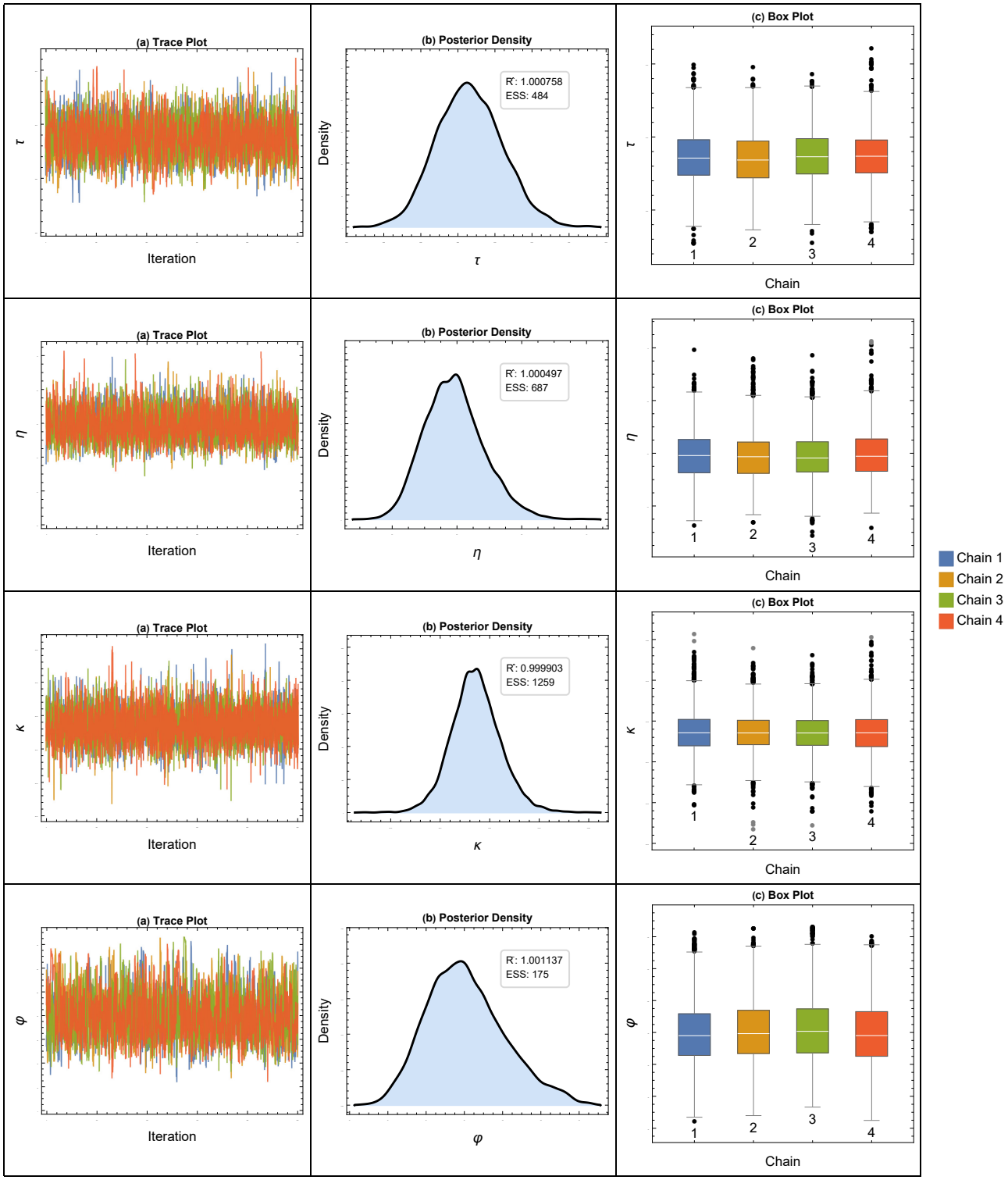

Figure 14. MCMC convergence diagnostics for the FEPW parameters under the Aarset dataset using the HMC–NUTS algorithm: (a) Trace plots, (b) marginal posterior density estimates, and (c) box plots across chains.

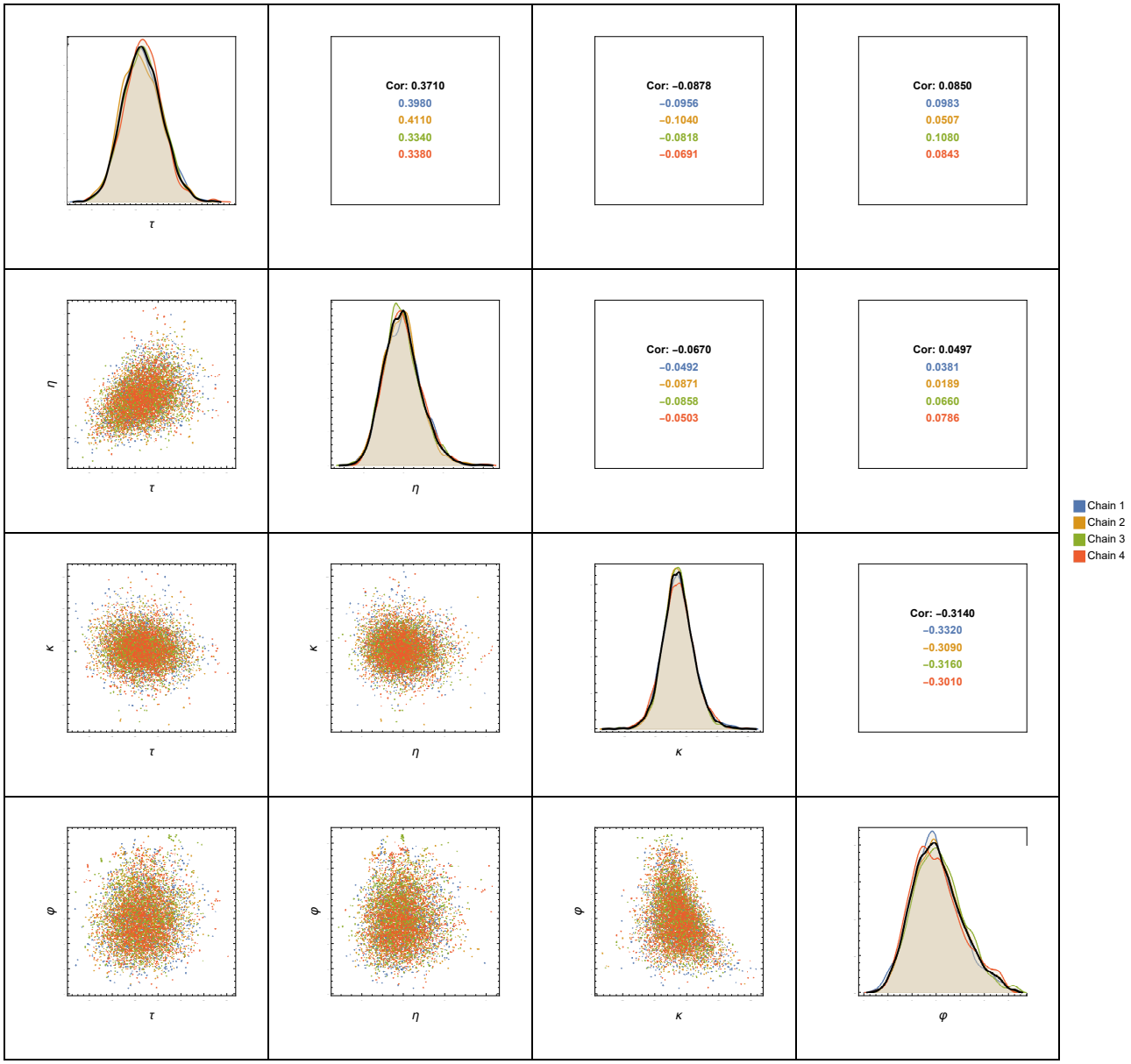

Figure 15. Pairwise scatter plot matrix of the FEPW posterior samples for the Aarset dataset, showing marginal posterior densities along the diagonal and pairwise dependence structures in the off-diagonal panels.

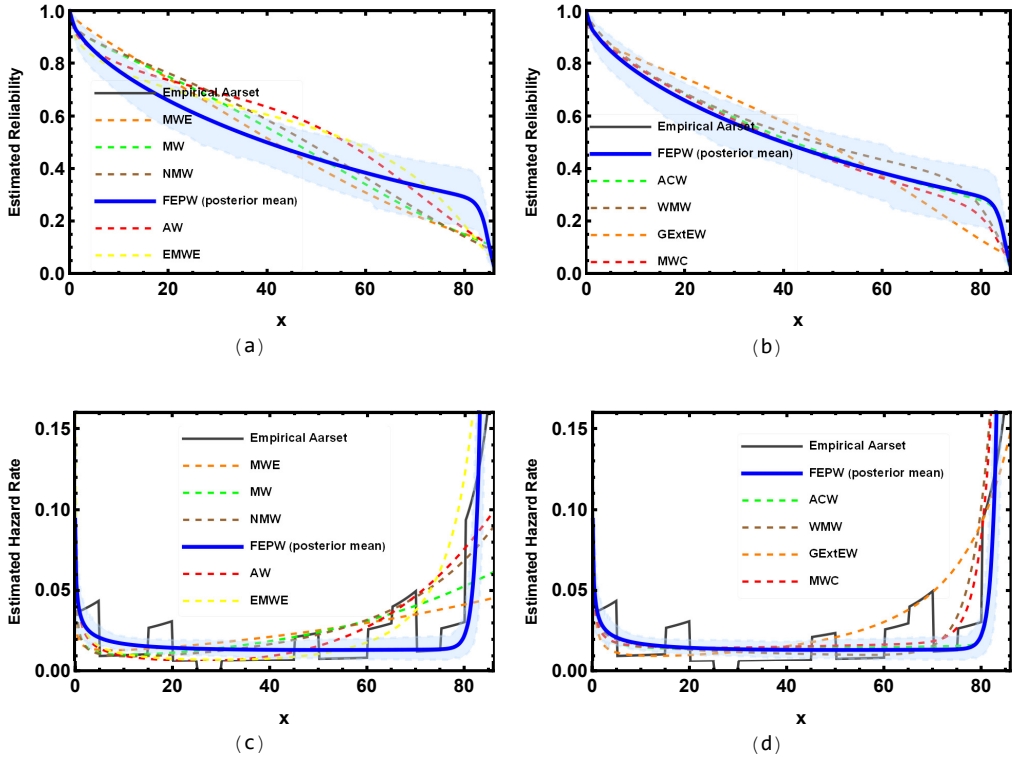

Figure 16. Graphical goodness-of-fit assessment for the Aarset dataset: (a) and (b) fitted reliability functions, and (c) and (d) estimated hazard rate functions for the FEPW model (posterior mean with 95% HPD band) and competing distributions.

6.3. Application 3: Early cable joint failures (Tang data)

The final application was based on the Tang dataset, which contains the failure times of early cable joints [33]. This dataset has been widely used in reliability studies to assess models capable of accommodating bathtub-shaped or other non-monotone hazard-rate behaviors.

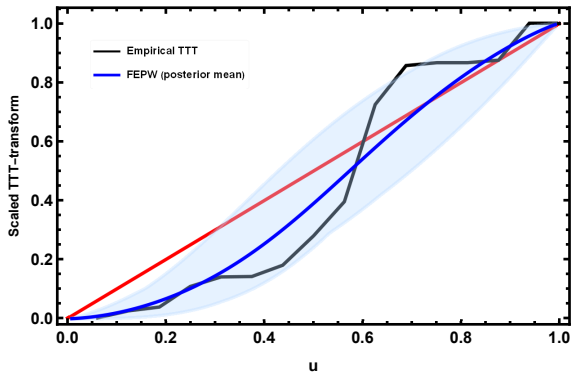

Figure 17. Empirical scaled TTT transform for the Tang dataset, together with the fitted FEPW posterior mean curve and its 95% HPD uncertainty band.

Before formal model fitting, I examined the qualitative behavior of the hazard rate using the scaled

Total Time on Test (TTT) transform shown in Figure 17. The empirical TTT curve exhibits an initial convex segment followed by a concave trend, which is consistent with a bathtub-shaped hazard-rate structure. The fitted FEPW posterior mean curve with its 95% HPD uncertainty band follows the empirical TTT pattern reasonably well. Motivated by this qualitative evidence, Table 12 reports the maximum likelihood estimates of the FEPW distribution and the competing models.

Table 12. Maximum likelihood estimates of the parameters for the FEPW distribution and competing models fitted to the Tang dataset.

Distribution	$\hat{\tau}$	$\hat{\eta}$	$\hat{\kappa}$	$\hat{\varphi}$	$\hat{\xi}$
MWE	1191.23	3.91135×10^{-4}	0.51866		
MW	0.01907	0.47624	2.47672×10^{-4}		
NMW	0.02262	0.42295	1.40118×10^{-4}		
FEPW	2.37124×10^{-4}	4.24584	5.11218×10^{-4}	0.54988	
AW	7.61671×10^{-5}	1.2133	0.03367	0.35559	
EMWE	176.137	0.43811	0.62437	2.57168×10^{-4}	
ACW	4.64941×10^{-4}	0.52307	0.32563	4.81046×10^{-7}	
WMW	0.02018	0.50974	6.85519×10^{-5}	0.6429	1.14266×10^{-3}
GExtEW	0.54301	0.08164	6.12821×10^{-5}	4.06106	1.63434
MWC	4.59746×10^{-10}	2.2334	7.78307×10^{-4}	0.02956	0.16865

To compare the fitted models more formally, Table 13 presents the goodness-of-fit statistics and information-theoretic criteria. The proposed FEPW distribution achieves the best performance with respect to the information criteria, yielding the smallest values of the negative log-likelihood ($-\ell = 128.922$), $\mathcal{I}_A$ (265.845), and $\mathcal{I}_B$ (268.935), and thus ranking first among the competing models under these criteria.

Table 13. Goodness-of-fit statistics and information-theoretic criteria for the FEPW distribution and competing models fitted to the Tang dataset. Superscripts denote model ranks from 1 (best) to 10 (worst).

Distribution	$-\ell$	$\mathcal{I}_A$	$\mathcal{I}_{Ac}$	$\mathcal{I}_B$	$\mathcal{I}_{HQ}$	D_n (p value)	W^2 (p-value)	A^2 (p value)
MWE	130.934^{8}	267.869^{3}	269.869^{3}	270.187^{3}	267.987^{3}	$0.1807\,(0.67302)^{10}$	$0.56476\,(0.67922)^{10}$	$0.09993\,(0.59092)^{10}$
MW	130.357^{6}	268.714^{5}	272.35^{4}	271.804^{4}	268.872^{5}	$0.16384\,(0.78364)^{6}$	$0.4549\,(0.79067)^{5}$	$0.0812\,(0.69159)^{5}$
NMW	130.162^{5}	270.324^{8}	276.324^{9}	274.187^{8}	270.522^{8}	$0.15704\,(0.82495)^{5}$	$0.46142\,(0.78394)^{7}$	$0.08209\,(0.68645)^{8}$
FEPW	128.922^{1}	265.845^{1}	269.481^{1}	268.935^{1}	266.003^{1}	$0.12669\,(0.95946)^{3}$	$0.3166\,(0.92419)^{2}$	$0.04747\,(0.89788)^{2}$
AW	131.553^{10}	271.107^{9}	274.743^{7}	274.197^{9}	271.265^{9}	$0.17862\,(0.68702)^{9}$	$0.48659\,(0.75798)^{8}$	$0.08202\,(0.68669)^{7}$
EMWE	131.038^{9}	270.076^{7}	273.712^{5}	273.166^{6}	270.234^{7}	$0.1678\,(0.75846)^{7}$	$0.54171\,(0.70201)^{9}$	$0.09691\,(0.60611)^{9}$
ACW	129.067^{2}	266.135^{2}	269.771^{2}	269.225^{2}	266.293^{2}	$0.12443\,(0.96537)^{2}$	$0.31762\,(0.92335)^{3}$	$0.0477\,(0.89671)^{3}$
WMW	129.106^{3}	268.212^{4}	274.212^{6}	272.075^{5}	268.41^{4}	$0.12213\,(0.97082)^{1}$	$0.3105\,(0.92915)^{1}$	$0.04509\,(0.91151)^{1}$
GExtEW	130.687^{7}	271.373^{10}	277.373^{10}	275.236^{10}	271.571^{10}	$0.17405\,(0.71755)^{8}$	$0.46039\,(0.78499)^{6}$	$0.08131\,(0.69097)^{6}$
MWC	129.857^{4}	269.713^{6}	275.713^{8}	273.576^{7}	269.911^{6}	$0.13129\,(0.94553)^{4}$	$0.38213\,(0.86446)^{4}$	$0.05333\,(0.86269)^{4}$

With respect to the distance-based goodness-of-fit measures, the FEPW distribution also remains highly competitive. In particular, it yields $D_n = 0.12669$ (rank 3), $W^2 = 0.05268$ (rank 2), and $A^2 = 0.35414$ (rank 2). Since smaller values of these statistics indicate closer agreement with the data, these results place the FEPW model among the top-performing candidates for the Tang dataset, especially in close comparison with the ACW and WMW distributions. The overall comparative ranking of the fitted models across the considered criteria is displayed in Figure 18.

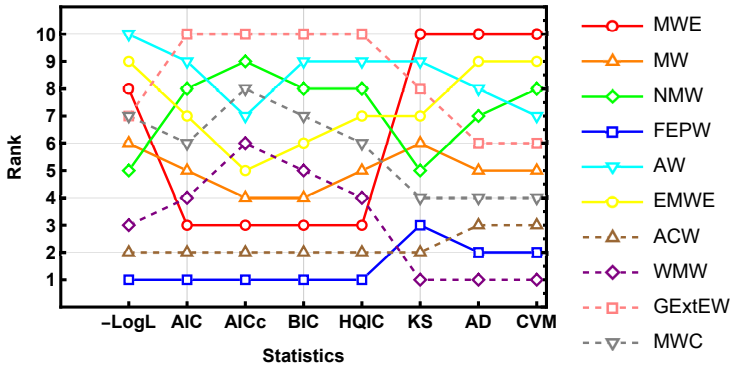

Figure 18. Comparative ranking plot of the fitted distributions across eight goodness-of-fit criteria for the Tang dataset.

Table 14 summarizes the Bayesian estimates obtained via the HMC–NUTS algorithm. The convergence diagnostics are satisfactory, with ˆR values very close to 1, and ESS values indicating acceptable sampling efficiency. This is visually supported by the stable trace plots and smooth, unimodal posterior densities in Figure 19, as well as by the pairwise dependence structure displayed in the scatter plot matrix of Figure 20. Finally, Figure 21 presents the fitted reliability and HRFs. The FEPW reliability curve (Figure 21(a)) with its 95% HPD uncertainty band follows the empirical reliability pattern reasonably well. Moreover, the estimated hazard rate in Figure 21(c) displays a bathtub-shaped pattern, characterized by relatively high initial failure rates, followed by a decline and a subsequent rise, which is consistent with the physical interpretation of early failures in cable joints.

Table 14. Maximum likelihood and Bayesian posterior estimates for the FEPW parameters under the Tang dataset with 95% confidence intervals, 95% HPD intervals, and convergence diagnostics ($\hat{R}$, ESS).

Parameter	MLEs	95% CI	Bayes	95% HPD	$\hat{R}$	ESS
$\hat{\tau}$	0.00024	[0.00019, 0.00028]	0.00022	[0.0001 , 0.00028]	0.99994	349
$\hat{\eta}$	4.25551	[-1.42499, 9.93601]	3.84894	[1.05498, 9.04911]	1.00019	309
$\hat{\kappa}$	0.00051	[-0.00014, 0.00117]	0.00052	[0.00014, 0.0011]	1.00047	640
$\hat{\varphi}$	0.54993	[0.21940, 0.88046]	0.5467	[0.29862, 0.86106]	1.00001	752

Finally, to assess the physical consistency of the fitted FEPW model, I examine the relationship between the HRF, $h(t)$, and the MRL function, $m(t)$, for the three datasets. Figure 22 displays these functions for the VETEs, Aarset, and Tang datasets, respectively. In all three cases, an inverse relationship is observed, which is consistent with reliability-theoretic expectations. In particular, during the useful-life phase, where the hazard rate remains relatively low and stable, the MRL stays comparatively high. In contrast, as the components approach the wear-out phase, and the hazard rate increases markedly toward the tail, the MRL declines toward zero. This counter-monotone behavior supports the ability of the FEPW distribution to represent the aging mechanism and progressive exhaustion of component lifetime across engineering settings.

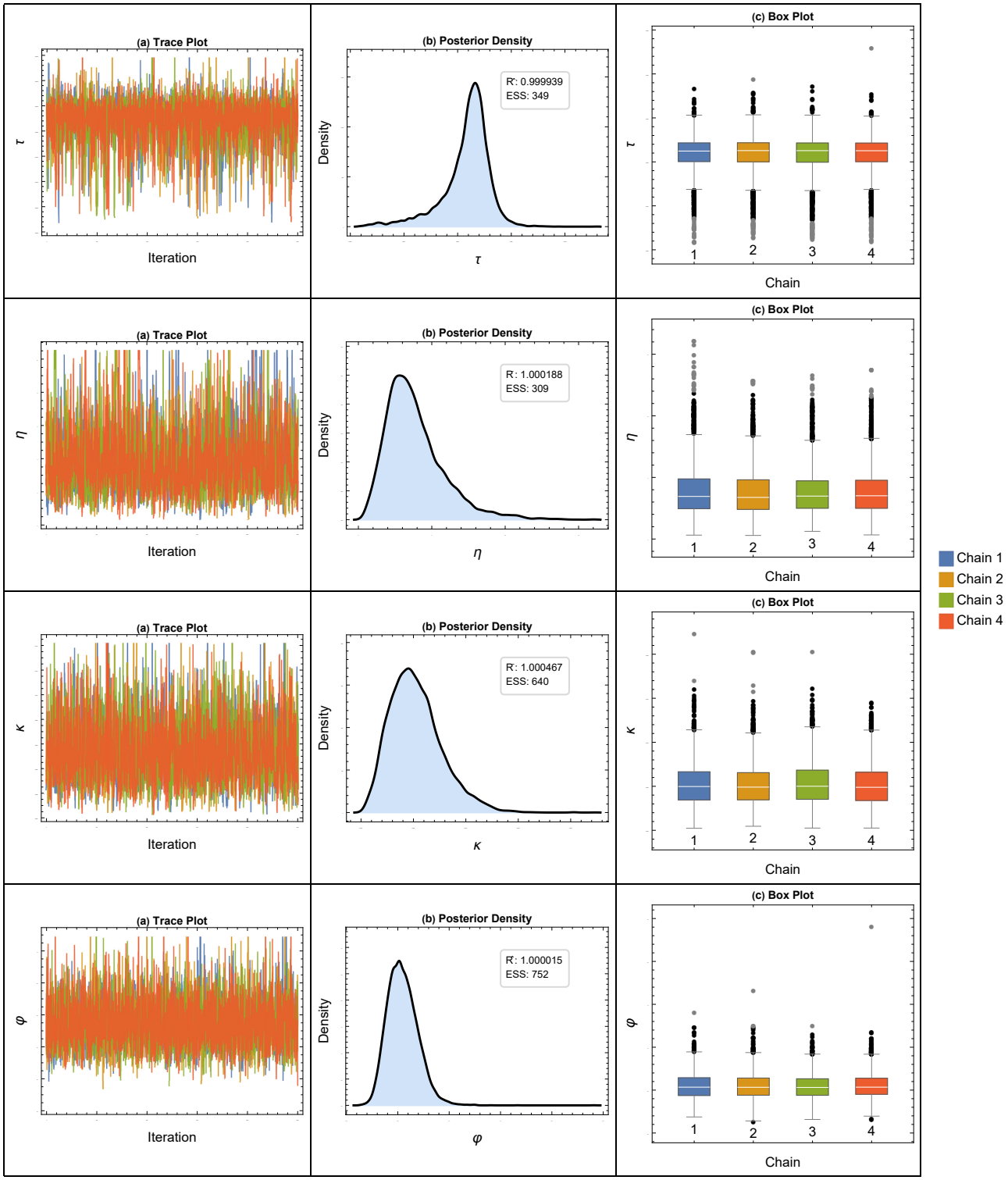

Figure 19. MCMC convergence diagnostics for the FEPW parameters under the Tang dataset using the HMC–NUTS algorithm: (a) Trace plots, (b) marginal posterior density estimates, and (c) box plots across chains.

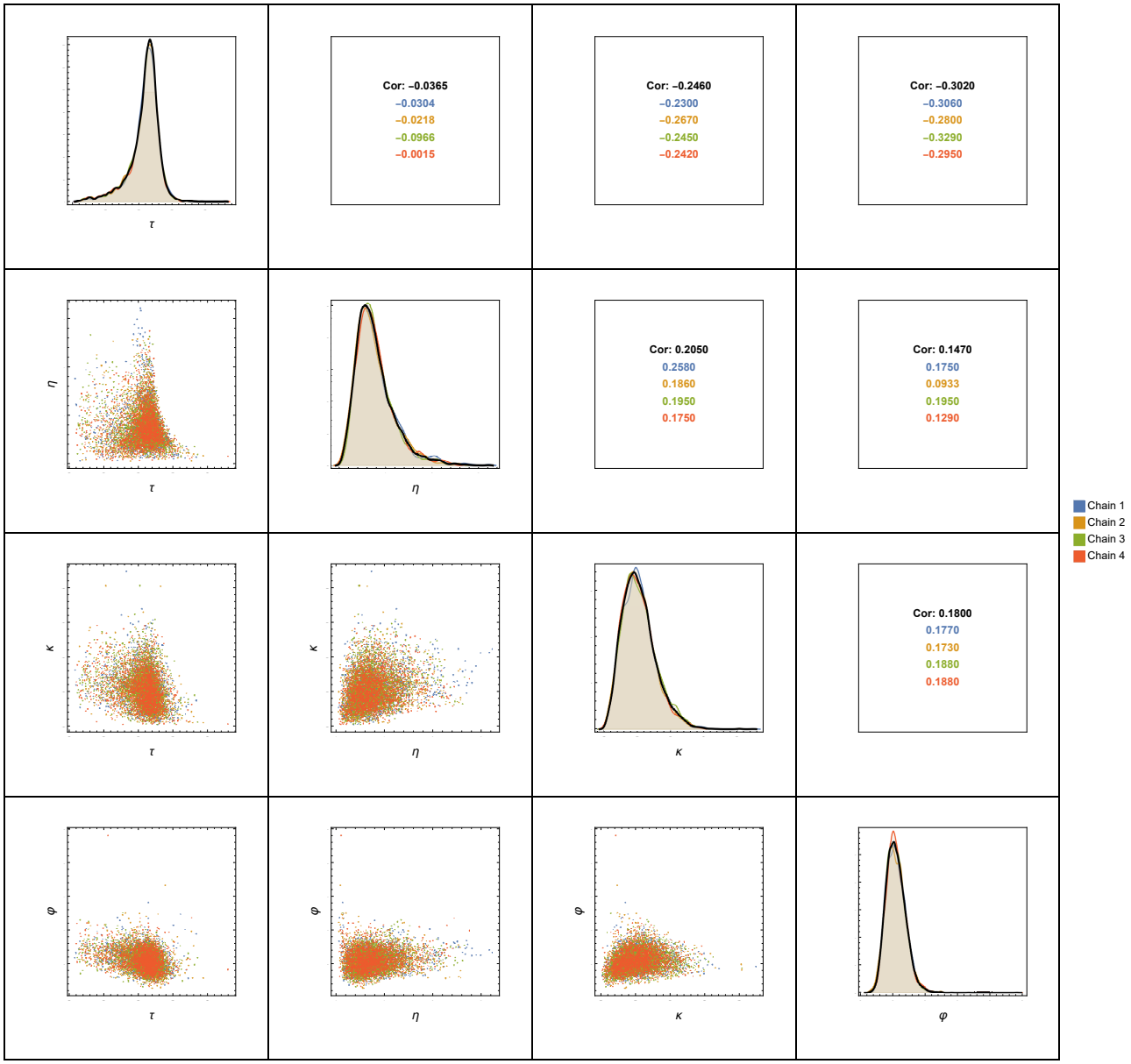

Figure 20. Pairwise scatter plot matrix of the FEPW posterior samples for the Tang dataset, showing marginal posterior densities along the diagonal and pairwise dependence structures in the off-diagonal panels.

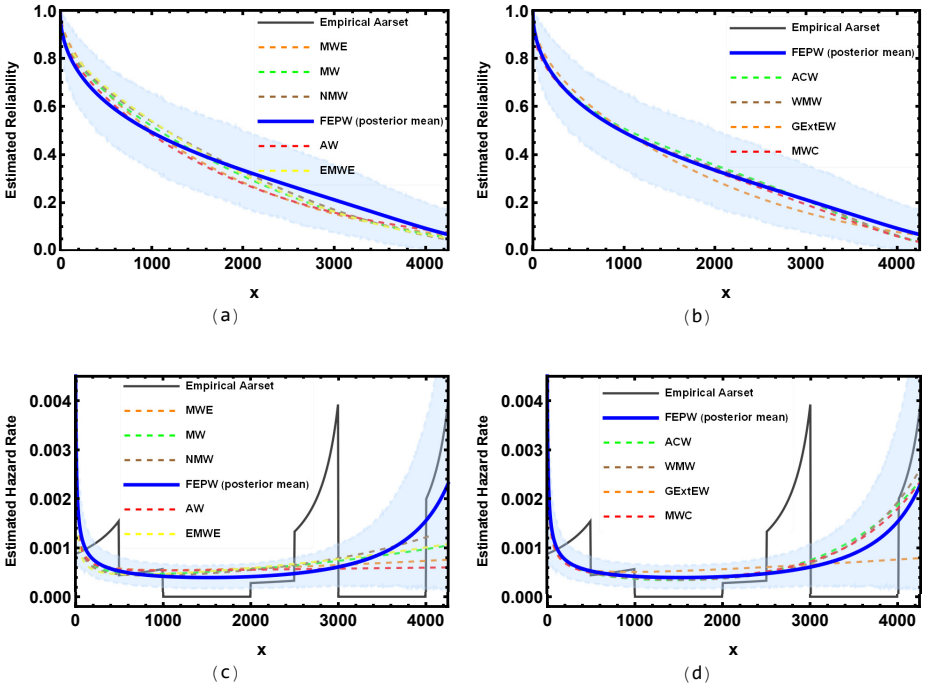

Figure 21. Graphical goodness-of-fit assessment for the Tang dataset: (a) and (b) fitted reliability functions, and (c) and (d) estimated hazard rate functions for the FEPW model (posterior mean with 95% HPD band) and competing distributions.

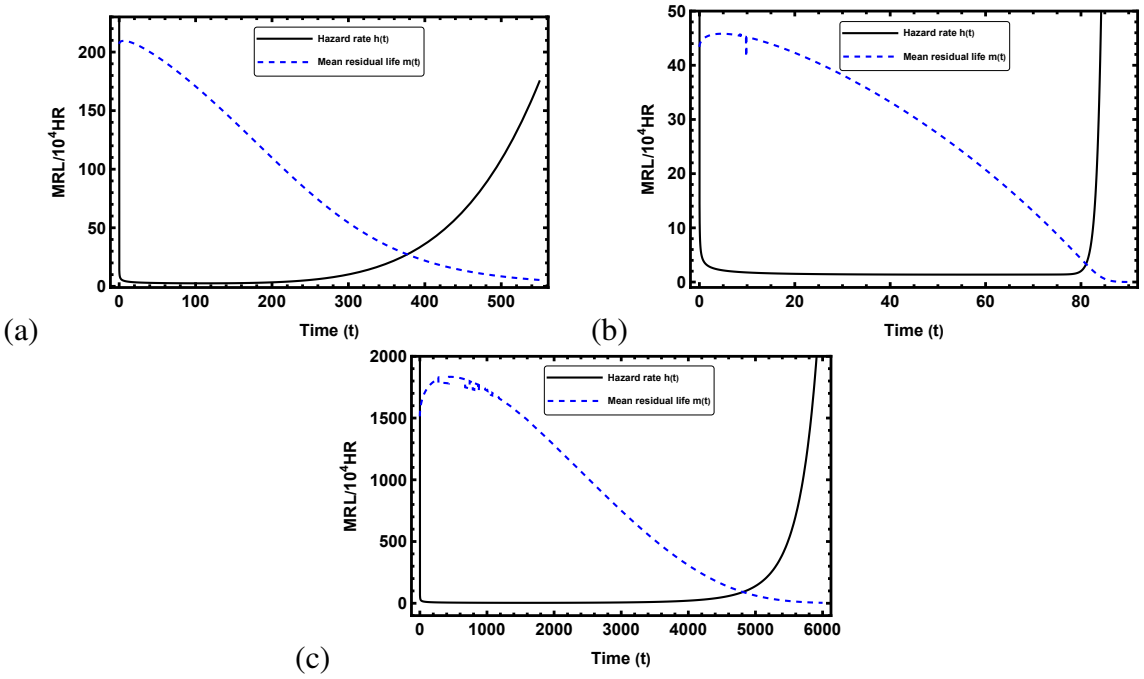

Figure 22. Graphical representation of the inverse relationship between the estimated hazard rate, $h(t)$, and mean residual life, $m(t)$, for the fitted FEPW distribution across the (a) VETEs, (b) Aarset, and (c) Tang datasets.

6.4. Sensitivity analysis

Table 15 reports a sensitivity analysis of the HMC–NUTS target acceptance rate $\delta \in \{0.9, 0.8, 0.75\}$ to assess the robustness of the posterior summaries and the diagnostic behavior of the sampler across the VETEs, Aarset, and Tang datasets. The major findings may be summarized as follows:

- **Relative stability of posterior means:** The posterior mean estimates of τ, η, κ, and φ remain reasonably stable across the examined values of δ for all datasets. This indicates that the central posterior summaries are not highly sensitive to moderate changes in the target acceptance rate, thus supporting the robustness of the posterior inference.
- **Convergence and sampling efficiency:** $\hat{R}$ remains close to 1 overall in all reported cases, indicating satisfactory convergence behavior across the examined settings. Moreover, the ESS is generally more favorable at $\delta = 0.9$, suggesting more efficient posterior exploration under this setting.
- **Effect on numerical stability:** A clear pattern is observed in the divergent transitions. As δ decreases from 0.9 to 0.8 and 0.75, the number of divergent transitions increases substantially. For the VETEs dataset, the total number of divergences rises from 6 at $\delta = 0.9$ to 26 at $\delta = 0.8$ and 72 at $\delta = 0.75$. For the Aarset dataset, the corresponding values increase from 93 to 508 and 807. For the Tang dataset, the total number of divergences increases from 264 at $\delta = 0.9$ to 1065 at $\delta = 0.8$ and 1578 at $\delta = 0.75$. This behavior is consistent with the role of δ in HMC–NUTS, since larger target acceptance rates typically imply smaller integration steps and therefore reduce numerical instability in regions of high posterior curvature.
- **Per-chain diagnostic behavior:** The reported divergences are distributed across all chains rather than being confined to a single chain. This suggests that the numerical difficulties are mainly linked to the overall posterior geometry rather than to an isolated issue in a single chain.

Conclusion: Overall, the sensitivity analysis shows that the posterior means are broadly robust with respect to moderate changes in δ, whereas the diagnostic behavior is more favorable at $\delta = 0.9$. In particular, this setting yields fewer divergent transitions while maintaining satisfactory $\hat{R}$ and ESS values. Therefore, $\delta = 0.9$ was retained in the final implementation.

Table 15. Sensitivity analysis of the HMC–NUTS target acceptance rate δ: posterior summaries, convergence diagnostics, and per-chain divergent transitions (Here, C_1, C_2, C_3, and C_4 denote the numbers of divergent transitions in Chains 1–4, respectively).

Dataset	δ	Parameter	Mean	$\hat{R}$	ESS	Per-chain divergences				Total divergences
						C_1	C_2	C_3	C_4	
VETEs	0.9	τ	0.00155	1.00034	447	1	1	4	0	6
		η	0.68753	1.00018	762					
		κ	0.00283	0.99994	467					
		φ	5.86373	1.00153	494					
	0.8	τ	0.00152	1.00019	431	8	6	7	5	26
		η	0.68138	1.00002	576					
		κ	0.00284	0.99993	656					
		φ	5.92076	1.00040	386					
	0.75	τ	0.00152	1.00151	286	21	16	12	23	72
		η	0.67781	1.00088	467					
		κ	0.00284	1.00075	496					
		φ	5.84356	1.00198	420					
Aarset	0.9	τ	0.00863	1.00076	484	23	25	19	26	93
		η	0.59133	1.00050	687					
		κ	0.01177	0.99990	1259					
		φ	80.812	1.00114	175					
	0.8	τ	0.00866	1.00072	156	141	133	128	106	508
		η	0.59590	1.00536	76					
		κ	0.01177	1.00033	678					
		φ	80.092	1.00444	69					
	0.75	τ	0.00847	1.00893	60	183	195	164	265	807
		η	0.58551	1.00689	53					
		κ	0.01177	1.00005	343					
		φ	77.914	1.00348	24					
Tang	0.9	τ	0.00022	0.99994	349	65	51	67	65	248
		η	3.84894	1.00019	309					
		κ	0.00052	1.00047	640					
		φ	0.5467	1.00001	752					
	0.8	τ	0.00022	1.00018	424	287	244	251	283	1065
		η	3.90421	1.00076	133					
		κ	0.00052	1.00212	409					
		φ	0.54793	1.00058	463					
	0.75	τ	0.00022	0.99998	344	427	410	415	326	1578
		η	3.91395	1.00076	129					
		κ	0.00052	1.00162	358					
		φ	0.54957	1.00012	536					

7. Conclusions

In this study, I introduced the Flexible Exponential Power-Weibull (FEPW) distribution, a novel four-parameter lifetime model constructed within a competing risks framework. By compounding the exponential power and Weibull distributions, the FEPW model offers a highly adaptable structure capable of capturing diverse hazard rate behaviors, including increasing, decreasing, unimodal, and, most notably, bathtub-shaped patterns with extended useful-life phases.

The significance of the FEPW distribution lies not only in its flexibility but also in its statistical robustness. Unlike many competing hybrid models constrained by rigid tail behaviors, the proposed FEPW framework effectively accommodates heavy-tailed data and varying degrees of kurtosis via the exponential power component. This structural advantage enables the precise modeling of systems

subject to random external shocks or extreme failure events (outliers), offering a distinct physical justification for its use in complex engineering contexts. Furthermore, I implemented a robust dual-estimation strategy, demonstrating that while the MLE is asymptotically efficient for large datasets, the Bayesian framework via HMC-NUTS provides superior stability and precision for small-sample scenarios.

Empirical applications to three distinct reliability datasets (VETEs, Aarset, and Tang) validated the practical superiority of the proposed model. The FEPW distribution consistently outperformed established Weibull extensions, such as the Modified Weibull Extension (MWE), Additive Chen-Weibull (ACW), and Generalized Extended Exponential-Weibull (GExtEW), across information-theoretic criteria and goodness-of-fit statistics. From a practitioner's perspective, the model's ability to accurately characterize the wear-out phase onset provides quality engineers with a reliable tool for optimizing preventive maintenance intervals and enhancing system reliability.

Despite these contributions, the formulation acknowledges a limitation regarding the assumption of independence between the latent failure modes (Exponential Power and Weibull components). In complex physical systems, failure mechanisms often exhibit dependency, which the current independent competing risks structure does not explicitly model.

In future research, I will address this limitation by incorporating dependence structures via copula functions to model the interaction between failure modes. Additionally, extending the FEPW model to bivariate and regression frameworks to accommodate covariates, as well as adapting the HMC-NUTS algorithm for censored data and accelerated life testing, represent promising directions for further investigation.

Use of Generative-AI tools declaration

The author declares he has not used Artificial Intelligence (AI) tools in the creation of this article.

Data availability

The raw datasets VETEs, Aarset, and Tang utilized in this study are publicly archived in the Zenodo repository and can be accessed at https://doi.org/10.5281/zenodo.19298256.

Conflict of interest

There is no conflict of interest declared by the author.

References

1. W. Weibull, A statistical distribution function of wide applicability, *J. Appl. Mech.*, **18** (1951), 293–297. http://dx.doi.org/10.1115/1.4010337
2. P. Kosky, R. Balmer, W. Keat, G. Wise, *Industrial engineering*, In: Exploring Engineering, Elsevier, 2021, 229–257. https://doi.org/10.1016/B978-0-12-815073-3.00011-9
3. W. Q. Meeker, L. A. Escobar, *Statistical methods for reliability data*, John Wiley & Sons, 1998.

4. B. Singh, An additive Perks–Weibull model with bathtub-shaped hazard rate function, *Commun. Math. Stat.*, **4** (2016), 473–493. http://dx.doi.org/10.1007/s40304-016-0096-z
5. M. K. Shakhatreh, A. J. Lemonte, G. M. Arenas, The log-normal modified Weibull distribution and its reliability implications, *Reliab. Eng. Syst. Saf.*, **188** (2019), 6–22. http://dx.doi.org/10.1016/j.ress.2019.03.014
6. B. Abba, H. Wang, H. S. Bakouch, A reliability and survival model for one and two failure modes system with applications to complete and censored datasets, *Reliab. Eng. Syst. Saf.*, **223** (2022), 108460. http://dx.doi.org/10.1016/j.ress.2022.108460
7. L. C. M. González, L. A. R. Picón, M. I. R. Borbón, H. Sohn, The Chen–Perks distribution: Properties and reliability applications, *Mathematics*, **11** (2023), 3001. http://dx.doi.org/10.3390/math11133001
8. B. Abba, H. Wang, M. Muhammad, H. S. Bakouch, A robust bathtub-shaped failure time model for a two-component system with applications to complete and censored reliability data, *Qual. Technol. Quant. M.*, **21** (2024), 309–339. http://dx.doi.org/10.1080/16843703.2023.2193771
9. A. U. Abdullahi, H. Wang, Y. Liu, Y. Qin, Robust failure time model with Bayesian inference and its application to reliability analysis, *Qual. Reliab. Eng. Int.*, 2025. http://dx.doi.org/10.1002/qre.3821
10. R. Jiang, D. N. P. Murthy, Reliability modeling involving two Weibull distributions, *Reliab. Eng. Syst. Saf.*, **47** (1995), 187–198. http://dx.doi.org/10.1016/0951-8320(94)00045-P
11. S. J. Almalki, J. Yuan, A new modified Weibull distribution, *Reliab. Eng. Syst. Saf.*, **111** (2013), 164–170. http://dx.doi.org/10.1016/j.ress.2012.10.018
12. B. Tarvirdizade, M. Ahmadpour, A new extension of Chen distribution with applications to lifetime data, *Commun. Math. Stat.*, **9** (2021), 23–38. http://dx.doi.org/10.1007/s40304-019-00185-4
13. T. T. Thach, R. Bris, An additive Chen–Weibull distribution and its applications in reliability modeling, *Qual. Reliab. Eng. Int.*, **37** (2021), 352–373. http://dx.doi.org/10.1002/qre.2740
14. B. Abba, H. Wang, A new failure times model for one and two failure modes system: A Bayesian study with Hamiltonian Monte Carlo simulation, *Proc. I. Mech. Eng. O-J. Risk Reliab.*, **238** (2024), 304–323. http://dx.doi.org/10.1177/1748006X221146367
15. B. Abba, J. Wu, M. Muhammad, A robust multi-risk model and its reliability relevance: A Bayes study with Hamiltonian Monte Carlo methodology, *Reliab. Eng. Syst. Saf.*, **250** (2024), 110310. http://dx.doi.org/10.1016/j.ress.2024.110310
16. N. Metropolis, A. W. Rosenbluth, M. N. Rosenbluth, A. H. Teller, E. Teller, Equation of state calculations by fast computing machines, *J. Chem. Phys.*, **21** (1953), 1087–1092. http://dx.doi.org/10.1063/1.1699114
17. W. K. Hastings, Monte Carlo sampling methods using Markov chains and their applications, *Biometrika*, **57** (1970), 97–109. http://dx.doi.org/10.1093/biomet/57.1.97
18. A. E. Gelfand, Gibbs sampling, *J. Amer. Statist. Assoc.*, **95** (2000), 1300–1304. https://doi.org/10.2307/2669775
19. R. M. Neal, *MCMC using Hamiltonian dynamics*, In: S. Brooks, A. Gelman, G. Jones, et al., Eds., Handbook of Markov Chain Monte Carlo, Florida: CRC Press, 2011, 113–162.

20. M. D. Hoffman, A. Gelman, The No-U-Turn sampler: Adaptively setting path lengths in Hamiltonian Monte Carlo, *J. Mach. Learn. Res.*, **15** (2014), 1593–1623.

21. M. Nishio, A. Arakawa, Performance of Hamiltonian Monte Carlo and No-U-Turn sampler for estimating genetic parameters and breeding values, *Genet. Sel. Evol.*, **51** (2019). https://doi.org/10.1186/s12711-019-0515-1

22. L. Devlin, M. Carter, P. R. Horridge, P. L. Green, S. Maskell, The No-U-Turn sampler as a proposal distribution in a sequential Monte Carlo sampler without accept/reject, *IEEE Signal Proc. Let.*, **31** (2024), 1089–1093. https://doi.org/10.1109/LSP.2024.3386494

23. D. Levy, M. D. Hoffman, J. Sohl-Dickstein, Generalizing Hamiltonian Monte Carlo with neural networks, *arXiv Preprint*, 2018. http://dx.doi.org/10.48550/arXiv.1711.09268

24. X. Meng, J. L. Beck, Y. Huang, H. Li, Adaptive meta-learning stochastic gradient Hamiltonian Monte Carlo simulation for Bayesian updating of structural dynamic models, *Comput. Method. Appl. M.*, **437** (2025), 117753. https://doi.org/10.1016/j.cma.2025.117753

25. M. Xie, Y. Tang, T. N. Goh, A modified Weibull extension with bathtub-shaped failure rate function, *Reliab. Eng. Syst. Saf.*, **76** (2002), 279–285. https://doi.org/10.1016/S0951-8320(02)00022-4

26. C. D. Lai, M. Xie, D. N. P. Murthy, A modified Weibull distribution, *IEEE T. Reliab.*, **52** (2003), 33–37. https://doi.org/10.1109/TR.2002.805788

27. M. G. M. Ghazal, A new extension of the modified Weibull distribution with applications for engineering data, *Probabilist. Eng. Mech.*, **74** (2023), 103523. https://doi.org/10.1016/j.probengmech.2023.103523

28. A. M. Sarhan, J. Apaloo, Exponentiated modified Weibull extension distribution, *Reliab. Eng. Syst. Saf.*, **112** (2013), 137–144. https://doi.org/10.1016/j.ress.2012.10.013

29. M. K. Shakhatreh, A. J. Lemonte, G. M. Cordeiro, On the generalized extended exponential–Weibull distribution: Properties and different methods of estimation, *Int. J. Comput. Math.*, **97** (2020), 1029–1057. https://doi.org/10.1080/00207160.2019.1605062

30. B. He, W. Cui, X. Du, An additive modified Weibull distribution, *Reliab. Eng. Syst. Saf.*, **145** (2016), 28–37. http://dx.doi.org/10.1016/j.ress.2015.08.010

31. N. Doganaksoy, G. Hahn, W. Meeker, Reliability analysis by failure mode, *Qual. Prog.*, **35** (2002), 47–52.

32. M. V. Aarset, How to identify a bathtub hazard rate, *IEEE T. Reliab.*, **R-36** (1987), 106–108. http://dx.doi.org/10.1109/TR.1987.5222310

33. Z. Tang, W. Zhou, J. Zhao, D. Wang, L. Zhang, H. Liu, et al., Comparison of the Weibull and the Crow–AMSAA model in prediction of early cable joint failures, *IEEE T. Power Deliver.*, **30** (2015), 2410–2418. http://dx.doi.org/10.1109/TPWRD.2015.2404926

A. Proofs of the properties of the FEPW distribution

This appendix provides detailed and rigorous proofs for the theorems concerning the statistical properties of the FEPW distribution stated in Section 3. The derivations rely on standard techniques in

mathematical statistics, including series expansions, integral transformations, and properties of special functions (notably the gamma and incomplete gamma functions).

A.1. Proof of Theorem 1: Moments

Proof. The r-th raw moment is defined as

$$\mu_r = \int_0^{+\infty} r\, x^{r-1}\, R(x;\Theta)\, \mathrm{d}x.$$

Substituting the RF $R(x;\Theta)$ from Eq (2.1) yields

$$\mu_r = r\, \mathrm{e} \int_0^{+\infty} x^{r-1}\, \mathrm{e}^{-\mathrm{e}^{(\tau x)^\eta}-(\kappa x)^\varphi}\, \mathrm{d}x.$$

To evaluate this, expand $\mathrm{e}^{-\mathrm{e}^{(\tau x)^\eta}}$ using a double Taylor series:

$$\mathrm{e}^{-\mathrm{e}^{(\tau x)^\eta}} = \sum_{i=0}^{+\infty}\sum_{j=0}^{+\infty} \frac{(-1)^i i^j \tau^{j\eta}}{i!\, j!} x^{j\eta}.$$

Substituting into the integral gives

$$\mu_r = r\, \mathrm{e} \sum_{i=0}^{+\infty}\sum_{j=0}^{+\infty} \frac{(-1)^i i^j \tau^{j\eta}}{i!\, j!} \int_0^{+\infty} x^{r+j\eta-1}\, \mathrm{e}^{-(\kappa x)^\varphi}\, dx.$$

The inner integral evaluates to $\frac{1}{\varphi \kappa^{r+j\eta}}\Gamma\left(\frac{r+j\eta}{\varphi}\right)$ via a change of variables $u = (\kappa x)^\varphi$, completing the proof. □

A.2. Proof of Theorem 2: Incomplete moments

Proof. The r-th incomplete moment is

$$\begin{aligned} I_m^r(v) &= \int_0^v t^r f(t;\Theta)\, dt \\ &= \mathrm{e} \int_0^v t^r \left(\eta\, \tau\, (\tau t)^{\eta-1}\, \mathrm{e}^{(\tau t)^\eta} + \kappa\, \varphi\, (\kappa t)^{\varphi-1}\right) \mathrm{e}^{-\mathrm{e}^{(\tau t)^\eta}-(\kappa t)^\varphi}\, dt. \end{aligned}$$

This splits into two integrals, $I_1 + I_2$. Expanding $\mathrm{e}^{-\mathrm{e}^{(\tau t)^\eta}}$ as above yields

$$I_m^r(v) = \mathrm{e} \sum_{i=0}^{+\infty}\sum_{j=0}^{+\infty} \frac{(-1)^i i^j \tau^{j\eta}}{i!\, j!}\, (I_1 + I_2)\,.$$

For I_1, further expand $\mathrm{e}^{(\tau t)^\eta} = \sum_{k=0}^{\infty} \frac{(\tau t)^{k\eta}}{k!}$, leading to

$$I_1 = \tau^\eta\, \eta \sum_{k=0}^{+\infty} \frac{\tau^{k\eta}}{k!} \int_0^v t^{r+(1+j+k)\eta-1}\, \mathrm{e}^{-(\kappa t)^\varphi}\, dt$$

$$= \sum_{k=0}^{+\infty} \frac{\tau^{(k+1)\eta}\ \eta}{k!\,\varphi\,\kappa^{r+(1+j+k)\eta}}\,\gamma_1\left(\frac{r+(1+j+k)\eta}{\varphi},\,(\kappa\,v)^{\varphi}\right).$$

For I_2,

$$\begin{aligned} I_2 &= \kappa^{\varphi}\,\varphi\int_0^{v} t^{r+j\eta+\varphi-1}\,\mathrm{e}^{-(\kappa\,t)^{\varphi}}\,dt \\ &= \frac{1}{\kappa^{r+j\eta}}\,\gamma_2\left(\frac{r+j\eta}{\varphi}+1,\,(\kappa\,v)^{\varphi}\right). \end{aligned}$$

Combining these completes the proof. □

A.3. Proof of Theorem 3: Mean residual life

Proof. The MRL is defined as:

$$\begin{aligned} \mu_X(t) &= \mathbb{E}[X-t \mid X>t] \\ &= \frac{1}{R(t;\Theta)}\int_t^{+\infty} R(x;\Theta)\,\mathrm{d}x \\ &= \mathrm{e}^{\mathrm{e}^{(\tau\,t)^{\eta}}+(\kappa\,t)^{\varphi}}\int_t^{+\infty}\mathrm{e}^{-\mathrm{e}^{(\tau\,x)^{\eta}}-(\kappa\,x)^{\varphi}}\,\mathrm{d}x. \end{aligned}$$

Expanding $\mathrm{e}^{-\mathrm{e}^{(\tau\,x)^{\eta}}}$ as in Appendix A.1 gives

$$\mu_X(t) = \mathrm{e}^{\mathrm{e}^{(\tau\,t)^{\eta}}+(\kappa\,t)^{\varphi}}\sum_{i=0}^{+\infty}\sum_{j=0}^{+\infty}\frac{(-1)^i\,i^j\,\tau^{j\eta}}{i!\,j!}\int_t^{+\infty} x^{j\eta}\,\mathrm{e}^{-(\kappa\,x)^{\varphi}}\,\mathrm{d}x.$$

The integral evaluates to $\frac{1}{\varphi\kappa^{j\eta+1}}\Gamma\left(\frac{j\eta+1}{\varphi},(\kappa t)^{\varphi}\right)$, completing the proof. □

A.4. Proof of Theorem 4: Rényi entropy

Proof. For order r ($r>0$, $r\neq 1$), the Rényi entropy is defined as

$$H_r(X) = \frac{1}{1-r}\,\log\int_0^{+\infty}[f(x;\Theta)]^r\,\mathrm{d}x.$$

Substituting the PDF yields

$$H_r(X) = \frac{1}{1-r}\,\log\int_0^{+\infty}\mathrm{e}^{r}\left[\eta\,\tau\,(\tau x)^{\eta-1}\,\mathrm{e}^{(\tau x)^{\eta}}+\kappa\,\varphi\,(\kappa\,x)^{\varphi-1}\right]^r\,\mathrm{e}^{-r\left(\mathrm{e}^{(\tau\,x)^{\eta}}+(\kappa\,x)^{\varphi}\right)}\,\mathrm{d}x.$$

Binomial expansion of the bracketed term gives

$$\begin{aligned} H_r(X) \;=\; & \frac{1}{1-r}\,\log\sum_{i=0}^{r}\binom{r}{i}\mathrm{e}^{r}\,\tau^{i\eta}\,\eta^{i}\,\kappa^{(r-i)\,\varphi}\,\varphi^{(r-i)} \\ & \times\int_0^{+\infty} x^{(\eta-\varphi)\,i+(\varphi-1)\,r}\,\mathrm{e}^{i(\tau\,x)^{\eta}-r\left(\mathrm{e}^{(\tau\,x)^{\eta}}+(\kappa\,x)^{\varphi}\right)}\,\mathrm{d}x. \end{aligned}$$

Further expansions of $e^{i(\tau x)^\eta}$ and $e^{-r\,e^{(\tau x)^\eta}}$ lead to

$$H_r(X) = \frac{1}{1-r}\log\sum_{j=0}^{+\infty}\sum_{k=0}^{+\infty}\sum_{l=0}^{+\infty}\sum_{i=0}^{r}\frac{\binom{r}{i}e^r(-1)^k i^j r^k k^l \tau^{(i+j+l)\eta}\eta^i \kappa^{(r-i)\varphi}\varphi^{(r-i)}}{j!\,k!\,l!}$$
$$\times\int_0^{+\infty} x^{(i+j+l)\eta+(r-i)\varphi-r}\,e^{-r(\kappa x)^\varphi}\,dx.$$

Evaluating the last integral using the gamma function yields the final expression. □

A.5. Proof of Theorem 5: Stress-strength reliability

Proof. Let $X \sim \text{FEPW}(\Theta_1)$ (strength) and $Y \sim \text{FEPW}(\Theta_2)$ (stress). The stress–strength reliability is

$$R_{SS} = P(X > Y) = \int_0^{+\infty} f_X(x;\Theta_1)\,F_Y(x;\Theta_2)\,dx.$$

Substitute the PDF and CDF, the R_{SS} can be expressed as follows:

$$R_{SS} = \int_0^{+\infty}\left(\eta_1\tau_1(\tau_1 x)^{\eta_1-1}e^{(\tau_1 x)^{\eta_1}} + \kappa_1\varphi_1(\kappa_1 x)^{\varphi_1-1}\right)e^{1-e^{(\tau_1 x)^{\eta_1}}-(\kappa_1 x)^{\varphi_1}}$$
$$\times\left(1-e^{1-e^{(\tau_2 x)^{\eta_2}}-(\kappa_2 x)^{\varphi_2}}\right)dx.$$

Applying integration by parts yields

$$R_{SS} = \int_0^{+\infty}\left(\eta_2\tau_2(\tau_2 x)^{\eta_2-1}e^{(\tau_2 x)^{\eta_2}} + \kappa_2\varphi_2(\kappa_2 x)^{\varphi_2-1}\right)$$
$$\times e^{2-e^{(\tau_1 x)^{\eta_1}}-e^{(\tau_2 x)^{\eta_2}}-(\kappa_1 x)^{\varphi_1}-(\kappa_2 x)^{\varphi_2}}\,dx.$$

Expanding the exponential terms and simplifying gives

$$R_{SS} = e^2\sum_{i=0}^{+\infty}\sum_{j=0}^{+\infty}\sum_{k=0}^{+\infty}\sum_{l=0}^{+\infty}\sum_{m=0}^{+\infty}\frac{(-1)^{i+k+l}i^j l^m\tau_1^{j\eta_1}\kappa_1^{k\varphi_1}\tau_2^{m\eta_2}}{i!\,j!\,k!\,l!\,m!}\,(I_1+I_2), \tag{A.1}$$

where,

$$I_1 = \tau_2^{\eta_2}\eta_2\int_0^{+\infty} x^{j\eta_1+k\varphi_1+(m+1)\eta_2-1}\,e^{(\tau_2 x)^{\eta_2}-(\kappa_2 x)^{\varphi_2}}\,dx$$
$$= \tau_2^{\eta_2}\eta_2\sum_{n=0}^{+\infty}\frac{\tau_2^{n\eta_2}}{n!}\int_0^{+\infty} x^{j\eta_1+k\varphi_1+(m+n+1)\eta_2-1}\,e^{-(\kappa_2 x)^{\varphi_2}}\,dx$$
$$= \sum_{n=0}^{+\infty}\frac{\tau_2^{(n+1)\eta_2}\,\eta_2}{n!\,\varphi_2\,\kappa_2^{j\eta_1+k\varphi_1+(m+n+1)\eta_2}}\Gamma\left(\frac{j\eta_1+k\varphi_1+(m+n+1)\eta_2}{\varphi_2}\right),$$

$$I_2 = \kappa_2^{\varphi_2}\varphi_2\int_0^{+\infty} x^{j\eta_1+k\varphi_1+\varphi_2+m\eta_2-1}\,e^{-(\kappa_2 x)^{\varphi_2}}\,dx$$
$$= \frac{1}{\kappa_2^{j\eta_1+k\varphi_1+m\eta_2}}\Gamma\left(\frac{j\eta_1+k\varphi_1+m\eta_2}{\varphi_2}+1\right).$$

Combining I_1 and I_2 provides the full expression for R_{SS}.

□

A.6. Proof of Theorem 6: Order statistics

For a random sample of size n from the FEPW distribution, the PDF of the k-th order statistic $X_{k:n}$ is

$$f_{k:n}(x;\Theta) = \frac{n!}{(k-1)!\,(n-k)!}\left[F(x;\Theta)\right]^{k-1}\left[1-F(x;\Theta)\right]^{n-k} f(x;\Theta).$$

Substituting the CDF and PDF expressions yields

$$\begin{aligned} f_{k:n}(x;\Theta) &= \frac{n!}{(k-1)!\,(n-k)!}\left(\eta\,\tau\,(\tau x)^{\eta-1}\,\mathrm{e}^{(\tau x)^{\eta}} + \kappa\,\varphi\,(\kappa\,x)^{\varphi-1}\right) \\ &\quad\times\left[1-\mathrm{e}^{1-\mathrm{e}^{(\tau x)^{\eta}}-(\kappa x)^{\varphi}}\right]^{k-1}\left[\mathrm{e}^{1-\mathrm{e}^{(\tau x)^{\eta}}-(\kappa x)^{\varphi}}\right]^{n-k+1}. \end{aligned}$$

By expanding $\left[1-\mathrm{e}^{1-\mathrm{e}^{(\tau x)^{\eta}}-(\kappa x)^{\varphi}}\right]^{k-1}$ and simplifying the resulting terms algebraically, the order statistics $X_{k:n}$ of the FEPW(Θ) distribution can be expressed as follows:

$$\begin{aligned} f_{k:n}(x;\Theta) &= \frac{n!}{(n-k)!}\left(\eta\,\tau\,(\tau x)^{\eta-1}\,\mathrm{e}^{(\tau x)^{\eta}} + \kappa\,\varphi\,(\kappa\,x)^{\varphi-1}\right) \\ &\quad\times\sum_{j=0}^{k-1}\frac{(-1)^{j}}{j!\,(k-j-1)!}\left[\mathrm{e}^{1-\mathrm{e}^{(\tau x)^{\eta}}-(\kappa x)^{\varphi}}\right]^{n-k+j+1}. \end{aligned}$$

Noting that $h(x;\Theta) = \eta\,\tau\,(\tau x)^{\eta-1}\,\mathrm{e}^{(\tau x)^{\eta}} + \kappa\,\varphi\,(\kappa\,x)^{\varphi-1}$ and $R(x;\Theta) = \mathrm{e}^{1-\mathrm{e}^{(\tau x)^{\eta}}-(\kappa x)^{\varphi}}$, the final expression follows, thereby completing the proof.

B. Elements of the Fisher information matrix for the FEPW distribution

$$\begin{aligned} \frac{\partial^2\ell(\Theta)}{\partial\tau^2} &= \frac{\eta^2}{\tau^2}\sum_{i=1}^{n}\frac{e^{(\tau x_i)^{\eta}}\,(\tau x_i)^{\,\eta}}{\left(\eta e^{(\tau x_i)^{\eta}}\,(\tau x_i)^{\,\eta}+\varphi\,(\kappa x_i)^{\,\varphi}\right)^2} \\ &\quad\times\left(\varphi\left(\eta+(3\eta-1)\,(\tau x_i)^{\,\eta}+\eta\,(\tau x_i)^{\,2\eta}-1\right)(\kappa x_i)^{\,\varphi}+\eta e^{(\tau x_i)^{\eta}}\left((\eta-1)\,(\tau x_i)^{\,\eta}-1\right)(\tau x_i)^{\,\eta}\right) \\ &\quad-\frac{\eta}{\tau^2}\sum_{i=1}^{n}\left(\eta+\eta\,(\tau x_i)^{\,\eta}-1\right)(\tau x_i)^{\,\eta}e^{(\tau x_i)^{\eta}}. \end{aligned}$$

$$\begin{aligned} \frac{\partial^2\ell(\Theta)}{\partial\tau\partial\eta} &= \frac{\eta}{\tau}\sum_{i=1}^{n}\frac{e^{(\tau x_i)^{\eta}}\,(\tau x_i)^{\,\eta}}{\left(\eta e^{(\tau x_i)^{\eta}}\,(\tau x_i)^{\,\eta}+\varphi\,(\kappa x_i)^{\,\varphi}\right)^2} \\ &\quad\times\Big[\,\varphi\,(\kappa x_i)^{\,\varphi}\left(2\left((\tau x_i)^{\,\eta}+1\right)+\eta\left(3\,(\tau x_i)^{\,\eta}+(\tau x_i)^{\,2\eta}+1\right)\log\left(\tau x_i\right)\right) \\ &\quad+\eta e^{(\tau x_i)^{\eta}}\,(\tau x_i)^{\,\eta}\left((\tau x_i)^{\,\eta}\left(\eta\log\left(\tau x_i\right)+1\right)+1\right)\Big] \\ &\quad-\frac{1}{\tau}\sum_{i=1}^{n}(\tau x_i)^{\,\eta}\left(\eta\left((\tau x_i)^{\,\eta}+1\right)\log\left(\tau x_i\right)+1\right)e^{(\tau x_i)^{\eta}}. \end{aligned}$$

$$\frac{\partial^2\ell(\Theta)}{\partial\tau\partial\kappa} = -\frac{\eta^2\varphi^2}{\kappa\tau}\sum_{i=1}^{n}\frac{(\tau x_i)^{\,\eta}\left((\tau x_i)^{\,\eta}+1\right)(\kappa x_i)^{\,\varphi}e^{(\tau x_i)^{\eta}}}{\left(\eta e^{(\tau x_i)^{\eta}}\,(\tau x_i)^{\,\eta}+\varphi\,(\kappa x_i)^{\,\varphi}\right)^2}.$$

$$\frac{\partial^2 \ell(\Theta)}{\partial \tau \partial \varphi} = -\frac{\eta^2}{\tau} \sum_{i=1}^{n} \frac{(\tau x_i)^{\eta} \left((\tau x_i)^{\eta} + 1\right) (\kappa x_i)^{\varphi} \left(\varphi \log(\kappa x_i) + 1\right) e^{(\tau x_i)^{\eta}}}{\left(\eta e^{(\tau x_i)^{\eta}} (\tau x_i)^{\eta} + \varphi (\kappa x_i)^{\varphi}\right)^2}.$$

$$\begin{aligned}\frac{\partial^2 \ell(\Theta)}{\partial \eta^2} &= \sum_{i=1}^{n} \frac{(\tau x_i)^{\eta} e^{(\tau x_i)^{\eta}}}{\left(\eta e^{(\tau x_i)^{\eta}} (\tau x_i)^{\eta} + \varphi (\kappa x_i)^{\varphi}\right)^2} \\ &\times \left[e^{(\tau x_i)^{\eta}} (\tau x_i)^{\eta} \left(\eta^2 (\tau x_i)^{\eta} \log^2(\tau x_i) - 1\right) \right. \\ &\left. + \varphi (\kappa x_i)^{\varphi} \log(\tau x_i) \left(2\left((\tau x_i)^{\eta} + 1\right) + \eta \left(3 (\tau x_i)^{\eta} + (\tau x_i)^{2\eta} + 1\right) \log(\tau x_i)\right)\right] \\ &- \sum_{i=1}^{n} (\tau x_i)^{\eta} \left((\tau x_i)^{\eta} + 1\right) \log^2(\tau x_i) e^{(\tau x_i)^{\eta}}.\end{aligned}$$

$$\frac{\partial^2 \ell(\Theta)}{\partial \eta \partial \kappa} = -\frac{\varphi^2}{\kappa} \sum_{i=1}^{n} \frac{(\tau x_i)^{\eta} (\kappa x_i)^{\varphi} \left(\eta \left((\tau x_i)^{\eta} + 1\right) \log(\tau x_i) + 1\right) e^{(\tau x_i)^{\eta}}}{\left(\eta e^{(\tau x_i)^{\eta}} (\tau x_i)^{\eta} + \varphi (\kappa x_i)^{\varphi}\right)^2}.$$

$$\frac{\partial^2 \ell(\Theta}{\partial \eta \partial \varphi} = -\sum_{i=1}^{n} \frac{(\tau x_i)^{\eta} (\kappa x_i)^{\varphi} \left(\eta \left((\tau x_i)^{\eta} + 1\right) \log(\tau x_i) + 1\right) \left(\varphi \log(\kappa x_i) + 1\right) e^{(\tau x_i)^{\eta}}}{\left(\eta e^{(\tau x_i)^{\eta}} (\tau x_i)^{\eta} + \varphi (\kappa x_i)^{\varphi}\right)^2}.$$

$$\begin{aligned}\frac{\partial^2 \ell(\Theta)}{\partial \kappa^2} &= \frac{\varphi^2}{\kappa^2} \sum_{i=1}^{n} \frac{(\kappa x_i)^{\varphi} \left(\eta(\varphi - 1) e^{(\tau x_i)^{\eta}} (\tau x_i)^{\eta} - \varphi (\kappa x_i)^{\varphi}\right)}{\left(\eta e^{(\tau x_i)^{\eta}} (\tau x_i)^{\eta} + \varphi (\kappa x_i)^{\varphi}\right)^2} \\ &- \frac{\varphi(\varphi - 1)}{\kappa^2} \sum_{i=1}^{n} (\kappa x_i)^{\varphi}.\end{aligned}$$

$$\begin{aligned}\frac{\partial^2 \ell(\Theta)}{\partial \kappa \partial \varphi} &= \frac{\varphi}{\kappa} \sum_{i=1}^{n} \frac{(\kappa x_i)^{\varphi} \left(\eta e^{(\tau x_i)^{\eta}} (\tau x_i)^{\eta} \left(\varphi \log(\kappa x_i) + 2\right) + \varphi (\kappa x_i)^{\varphi}\right)}{\left(\eta e^{(\tau x_i)^{\eta}} (\tau x_i)^{\eta} + \varphi (\kappa x_i)^{\varphi}\right)^2} \\ &- \frac{1}{\kappa} \sum_{i=1}^{n} (\kappa x_i)^{\varphi} \left(\varphi \log(\kappa x_i) + 1\right).\end{aligned}$$

$$\begin{aligned}\frac{\partial^2 \ell(\Theta)}{\partial \varphi^2} &= \sum_{i=1}^{n} \frac{(\kappa x_i)^{\varphi} \left(\eta e^{(\tau x_i)^{\eta}} (\tau x_i)^{\eta} \log(\kappa x_i) \left(\varphi \log(\kappa x_i) + 2\right) - (\kappa x_i)^{\varphi}\right)}{\left(\eta e^{(\tau x_i)^{\eta}} (\tau x_i)^{\eta} + \varphi (\kappa x_i)^{\varphi}\right)^2} \\ &- \sum_{i=1}^{n} (\kappa x_i)^{\varphi} \log^2(\kappa x_i).\end{aligned}$$